

國立交通大學
應用數學系
數學建模與科學計算
碩士班

碩士論文

光子晶體雷射耦合波理論之研究



*Study of Photonic Crystal Lasers by Coupled Wave
Theory*

研究生：郭訓利

指導教授：賴明治 教授

盧廷昌 教授

中華民國一百年十月

光子晶體雷射耦合波理論之研究

Study of Photonic Crystal Lasers by Coupled Wave Theory

研究生：郭訓利

Student : Hsun-Li Kuo

指導教授：賴明治

Advisors : Ming-Chih Lai

盧廷昌

Tien-Chang Lu



A thesis

Submitted to Institute of Mathematical Modeling and Scientific Computing

College of Science

National Chiao Tung University

In partial Fulfillment of the Requirements

for the Degree of Master

in

Mathematical Modeling and Scientific Computing

October 2011

Hsinchu, Taiwan, Republic of China

中華民國一百年十月

光子晶體雷射耦合波理論之研究

研究生：郭訓利

指導教授：賴明治 教授

盧廷昌 教授

國立交通大學 應用數學系數學建模與科學計算碩士班

摘要

本篇論文主旨在利用耦合波理論探討在四方晶格以及三角晶格結構下造成光子晶體雷射於橫向電場極化之分析。用來描述二維光學耦合的四方晶格模型是由八個布拉格衍射的耦合平面波組合而成的；而用來描述二維光學耦合的三角晶格模型是由六個布拉格衍射的耦合平面波組合而成的。根據光子晶體的布拉格理論，光子晶體必須滿足特定的布拉格繞射條件才能產生雷射。由於面射型光子晶體的特性，我們特別著重於在 Γ 點能帶的研究。共振頻率偏差和閾值增益的振盪模式在週期性圓孔晶格的情況下已經被探討。這些諧振模式的空間強度分佈也被計算。我們探討了耦合強度對於閾值增益和頻率偏差的影響。最後，我們考慮正方晶格和三角晶格面射型光子晶體雷射的輻射損失。這論文有助於我們了解正方晶格和三角晶格面射型光子晶體雷射的特性。

Study of Photonic Crystal Lasers by Coupled Wave Theory

Student : Hsun-Li Kuo

**Advisor: Ming-Chih Lai
Tien-Chang Lu**

Institute of Mathematical Modeling and Scientific Computing
National Chiao-Tung University

Abstract

In this thesis, we investigated the coupled wave analysis for square lattice and triangular lattice of photonic crystal (PC) lasers with transverse electric polarization. A model for square lattice consisting of eight plane waves coupled by Bragg diffraction is used to describe two-dimensional optical coupling. A model for triangular lattice consisting of six plane waves coupled by Bragg diffraction is used to describe two-dimensional optical coupling. Based on the Bragg diffraction theory for PCs period structure, the lasing behavior could only be happened when the Bragg condition is satisfied. Our studies are especially focused on the band edge at Γ point because of the characteristic of surface emitting condition. The resonant frequency deviation and threshold gain for the modes of oscillation have been determined for the case of index periodicity with a lattice of circular holes. The spatial intensity distributions of these resonant modes have also been calculated. We have investigated that the influence of coupling strength is to the threshold gain and frequency deviation. Finally, we consider the radiation loss for square lattice and triangular lattice of PCSELS. This thesis helped us to understand the characteristics of PCSELS for square lattice and triangular lattice.

誌謝

在交大碩士班兩年多的日子，現在即將就要結束了，這個碩士班的兩年多將會是我一輩子難以忘懷的回憶，在這裡有很多特別的經歷。

首先，我想要感謝的人就是我的共同指導老師 盧廷昌老師，老師讓我看到做研究所需要的態度與直覺，老師總是可以看到研究背後的意義。再來要感謝的也是我的指導老師 賴明治老師，由於有老師的支持讓我可以全心全力的做研究，不用弄得像熱鍋的螞蟻、兩頭燒的蠟燭。

在這我最要感謝的是翁鵬翔學長，翁翁學長總是不厭其煩的跟我討論研究上面的問題，在我迷惘的時候指點我研究的方向。也要感謝板弟學長在最後的這段日子裡，幫我修改我論文錯誤的部分，並且總是很有耐心的幫助我。另外感謝陳冠羽學長在我程式或是數學方面有問題的時候，總是可以給我適時的幫助。

碩士班同學啟豪、孫總、小蔣、芷萱、淑娟、志峰、佑慶、思維、just、羿綦、大寶、阿國、肉哥、jolin...，很高興可以認識大家，跟大家一起玩的日子很有趣，想念一起吃包子的日子，現在大家都已經各奔東西了，下次在聚在一起的時候不知道是何時了。學弟皇智、治成，有你們的幫忙與協助，讓我的實驗更加順利以及不同的樂趣。特別感謝我的好朋友家棋、智堯、靜宜跟瑞翔，在我低潮的時候有你們的陪伴讓我度過那個時期。

最後要感謝我的家人，你們總是無條件在我背後默默支持我，每次疲憊回去你們的安慰與鼓勵，總是讓我又有繼續努力的原動力!現在即將要踏入人生的另一個階段，真的非常感謝你們大家，我會再繼續往前進的。

Contents

Abstract (in Chinese)	I
Abstract (in English)	II
Acknowledgement	III
Contents	IV
Figure Contents	VI

Chapter 1 Introduction

1.1 Laser.....	1
1.2 Bragg diffraction in 2D Photonic Crystal.....	5
1.3 Outline of the thesis.....	10
References.....	11

Chapter 2 Fundamentals of Photonic Crystal Surface Emitting Lasers

Introduction.....	13
2.1.1 Couple-wave theory for square lattice.....	14
2.1.2 Finite difference method for square lattice.....	22
2.2.1 Couple-wave theory for triangular lattice.....	25
2.2.2 Finite difference method for triangular lattice.....	31
References.....	34

Chapter 3 Simulation Results of Photonic Crystal Surface Emitting Lasers

Numerical results.....	35
3.1.1 Mode spectra and mode patterns for square lattice.....	36
3.1.2 Threshold gain as a function of hole filling factor for square lattice.....	42
3.2.1 Mode spectra and mode patterns for triangular lattice.....	46
3.2.2 Threshold gain as a function of hole filling factor for triangular lattice.....	51
References.....	56

Chapter 4 Conclusion.....57
Appendix.....59

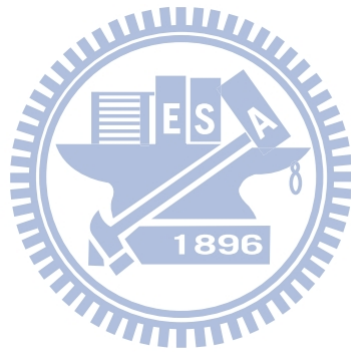


Figure contents

Fig 1.1	(a)The schematic diagram of an edge emitting laser (b) The schematic diagram of a vertical-cavity surface emitting laser (c)The schematic diagram of a photonic crystal surface emitting laser.....4
Fig 1.2	(a) The different band edges of triangular lattice photonic crystal in the band diagram (b) Schematic diagram of reciprocal space.....5
Fig. 1.3	Wave vector diagram at point (A)M1 (B)K1 (C) Γ 2 (D) M2, k_i and k_d indicate incident and diffracted light wave.....8
Fig. 1.4	The wave vector diagram at point Γ 2,K2,M3 in vertical direction.....9
Fig. 2.1	Schematic diagram of the polarization direction of wave.....13
Fig. 2.2	(a) Square lattice photonic crystal structure (b) Schematic diagram of eight propagation waves in square reciprocal lattice photonic crystal structure.....14
Fig. 2.3	Diffraction diagram for each coupling constant for square lattice. White arrows indicate pairs of wave vectors and black arrows indicate the corresponding reciprocal lattice vectors.....17
Fig. 2.4	Schematic diagram for square lattice for the finite difference method. The target of calculations is carried out at the positions of the white dots by using the complex amplitudes of the neighboring black dots.....24
Fig 2.5	(a) Triangular lattice photonic crystal structure (b) Schematic diagram of six propagation waves in triangular reciprocal lattice photonic crystal structure.....25
Fig. 2.6	Diffraction diagram for each coupling constant for triangular lattice. White arrows indicate pairs of wave vectors and black arrows indicate the corresponding reciprocal lattice vectors.....27

Fig. 2.7 Schematic diagram for triangular lattice for the finite difference method. The target of calculations is carried out at the positions of the white dots by using the complex amplitudes of the neighboring black dots.....33

Fig. 3.1 Band structure for square lattice photonic crystal with TE polarization.....38

Fig. 3.2 The detailed band structure in the proximity of the Γ - point for square lattice.....38

Fig 3.3 (a) Threshold gain as a function of frequency deviation from the Bragg condition for square lattice (b) Magnified plot for modes $N = -1$, and (c) for $N=1$39

Fig 3.4 (a-d) Mode pattern for square lattice for the fundamental modes (A, B, and E), respectively, (e-f) spatial intensity distributions A_0 and B_0 , and (g-j) mode pattern for the higher order modes.....40,41

Fig 3.5 Coupling constants as a function of hole filling factor for square lattice.....42

Fig 3.6 The frequency deviation as a function of hole filling factor of the fundamental modes A, B and E for square lattice for considering surface emission $\kappa_0 \neq 0$44

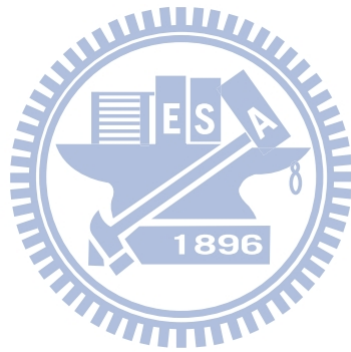
Fig 3.7 The threshold gain as a function of hole filling factor of the fundamental modes A, B and E for square lattice for considering surface emission $\kappa_0 \neq 0$44

Fig 3.8 The frequency deviation as a function of hole filling factor of the fundamental modes A, B and E for square lattice for zero surface emission $\kappa_0 = 0$45

Fig 3.9 The threshold gain as a function of hole filling factor of the fundamental

modes A, B and E for square lattice for zero surface emission $\kappa_0 = 0$	45
Fig. 3.10 Band structure for triangular lattice photonic crystal with TE polarization.....	48
Fig. 3.11 The detailed band structure in the proximity of the Γ - point for triangular lattice.....	48
Fig 3.12 Threshold gain as a function of frequency deviation from the Bragg condition for triangular lattice.....	49
Fig 3.13 (a-f)Mode pattern for triangular lattice for the fundamental modes (A, B, C, and D), respectively and (g-j) mode pattern for the higher order modes.....	49,50
Fig 3.14 Coupling constants as a function of hole filling factor for triangular lattice.....	51
Fig 3.15 The frequency deviation as a function of hole filling factor of the fundamental modes A, B, C and D for triangular lattice for considering surface emission $\kappa_0 \neq 0$	54
Fig 3.16 The threshold gain as a function of hole filling factor of the fundamental modes A, B, C and D for triangular lattice for considering surface emission $\kappa_0 \neq 0$	54
Fig 3.17 The frequency deviation as a function of hole filling factor of the fundamental modes A, B, C and D for triangular lattice for considering surface emission $\kappa_0 = 0$	55
Fig 3.18 The threshold gain as a function of hole filling factor of the fundamental modes A, B, C and D for triangular lattice for considering surface	

emission $\kappa_0 = 0$ 55



Chapter 1

Introduction

1.1 Laser

The concept of laser made by the Schawlow and Townes since 1960 [1] has caused considerable interest in the scientific community. The first ruby laser system made by Maiman in 1960 [2]. Then in 1962, gallium arsenide (GaAs) semiconductor laser is also immediately appear [3-5]. Semiconductor laser due to small size, long life and high stability has been widely applied in many different areas, such as optical fiber communication, optical storage and laser printing, molecular spectroscopy and biomedicine, military and blue-ray DVD, entertainment purposes and so on. Laser system is the elementary combination of the pumping source, the gain material, the optical cavity and the output coupler. The principle of operation is the input electricity or light of the pumping source can make the electronic absorption in the gain material and transition to excited state. Until the conduction band electron concentration attain to the population inversion and the electricity holes in the valence band combine into a large number of electron-hole pairs and emit photons, in order to achieve stimulated emission of the state and the optical cavity can limit to photon, choose the operating mode and to repeat the above process to achieve laser gain effect [6].

Laser can be divided into two classes by the direction of emission : edge emitting laser (EEL) and surface emitting laser (SEL). The laser light of edge emitting laser propagates parallel to the wafer surface of the semiconductor chip. Edge emitting laser is reflected or coupled out at a cleaved edge. The light of surface-emitting lasers propagates in the direction perpendicular to the semiconductor wafer surface.

Edge emitting laser (EEL)

Edge-emitting lasers are the original and still very widely used form of semiconductor lasers. Their resonator length is typically between a few hundred micrometers and a few millimeters. This is sufficient for reaching a high gain, so that an edge emitting laser may lase even if the resonator losses are fairly high. The laser beam within the edge emitting laser structure is guided in a waveguide structure. Typically, one uses a double heterostructure, which restricts the generated carriers to a narrow region and at the same time serves as a waveguide for the optical field, as shown in Fig 1.1(a). This arrangement leads to a low threshold pump power and a high efficiency.

Surface emitting laser (SEL)

There are several advantages to producing surface emitting lasers, in contrast to the production process of edge-emitting lasers. Edge-emitters cannot be tested until the end of the production process. If the edge-emitter does not function properly, whether due to bad contacts or poor material growth quality, the production time and the processing materials have been wasted. However, surface emitting lasers can be tested at several stages throughout the process to check for material quality and processing issues. Additionally, because surface emitting lasers emit the beam perpendicular to the active region of the laser as opposed to parallel as with an edge emitter. Furthermore, even though the surface emitting laser production process is more labor and material intensive, the yield can be controlled to a more predictable outcome. There are three common kind of surface emitting lasers that is vertical cavity surface emitting laser (VCSEL), as shown in Fig 1.1(b), distributed feedback laser (DFB) and photonic crystal surface emitting laser (PCSEL). Here, we mainly discuss the PCSEL.

Photonic Crystal Surface Emitting Laser (PCSEL)

Fig 1.1(c) shows the schematic diagram of a GaN-based PCSEL devices. The two-dimensional (2D) photonic crystal (PC) surface emitting laser is based on multidirectionally distributed feedback effect near the band edges in a 2D PC structure, which has potential for high-power and single mode surface-emitting lasers. PCs with photonic band gaps for photons have many advantages in arbitrarily controlling the light emission and propagation and can be utilized to realize various new optical devices. By varying the lattice constant of the PC pattern, different lasing wavelengths corresponding to different band edges are demonstrated. PCSEL utilizing 2D distributed feedback mechanism has been attracted much attention and widely researched during past decades [7-13]. PCSELS have many advantageous characteristics such as single mode operation in a large lasing area, a symmetric beam shape and a low divergence angle. Numerical studies have attempted to explain the distributed feedback mechanism for PCSELS by using different theoretical methods. Sakoda et al. used group-velocity anomaly to evaluate lasing threshold by the plane wave expansion method (PWEM) [14]. Lee et al. investigated the quality factor near band edges of finite-size photonic crystals (PCs) by the finite-difference time-domain (FDTD) method [15]. Sakai et al. calculated the threshold gain deviated from the Bragg frequency for square PCs by using the coupled wave theory [16-17]. Nojima proposed the multiple scattering method (MSM) to calculate lasing behaviors in PC lattice atoms with optical gains [18]. There are different advantages and limitations while using these theoretical methods to calculate characteristics of PC lasers. For example, the 2D PWEM better applies to the infinite PC structure, which is usually not the case for actual devices. FDTD method consumes numerous computer resources and calculation time to simulate the finite domain structure.

On the contrary, coupled wave theory has many advantages such as less

calculation time and capability in providing more accurate solutions to modify the designs. Therefore, the purpose of this thesis is to investigate the different parameters of the square lattice and triangular lattice PC including the influence of the coupling constant to the threshold gain and the frequency deviation at different band-edge modes.

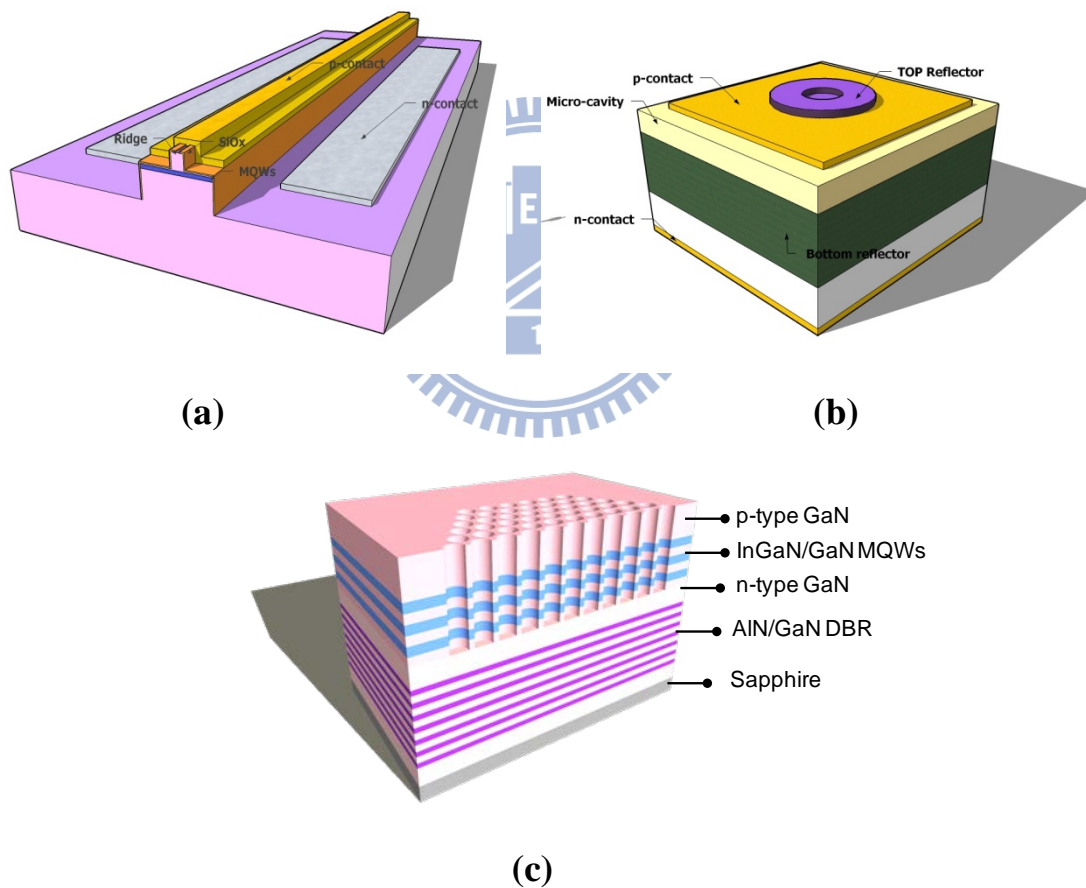


Fig 1.1 (a)The schematic diagram of an edge emitting laser (b) The schematic diagram of a vertical-cavity surface emitting laser (c)The schematic diagram of a photonic crystal surface emitting laser

1.2 Bragg diffraction in 2D Photonic Crystal_{[8][19]}

A band diagram of a triangular-lattice photonic crystal shows in Fig. 1.1(a). The points (A), (B), (C), and (D) are the points M1, K1, Γ 2, and M2, respectively. The reciprocal space of the structure is a space combined by hexagons. A schematic diagram of a reciprocal space shows in Fig. 1.1(b). The K1 and K2 are the Bragg vectors with the same magnitude, $|K|=2\pi/a$, where a is the lattice constant of the photonic crystal. Consider the transverse modes in the 2-D photonic crystal structure, the diffracted light wave from the structure must satisfy the relationship :

$$k_d - k_i = \Delta k = q_1 K_1 + q_2 K_2, \quad (q_1, q_2 = 0, \pm 1, \pm 2, \dots) \quad (1.1)$$

$$\omega_d = \omega_i \quad (1.2)$$

where k_d is xy -component wave vector of diffracted light wave, k_i is xy -component wave vector of incident light wave, q_1, q_2 is order of coupling, ω_d is

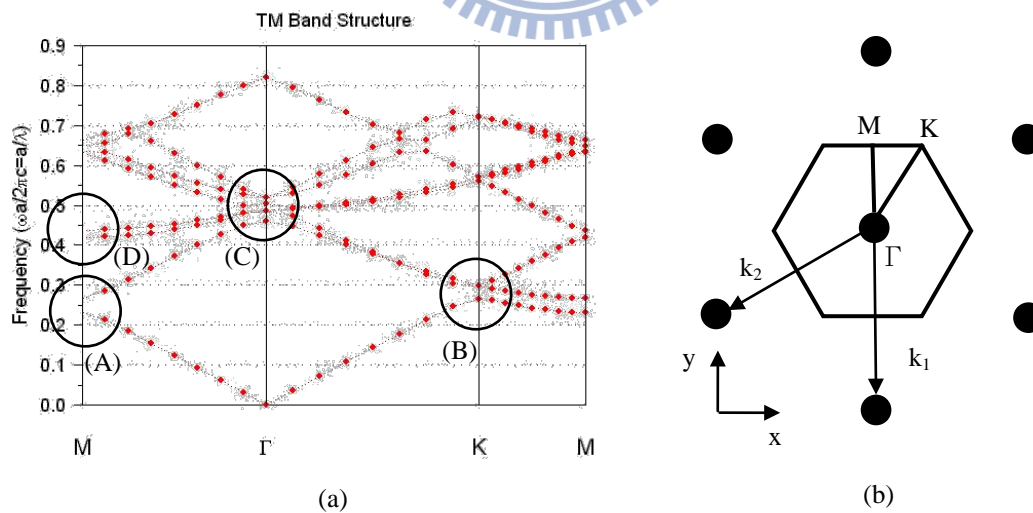
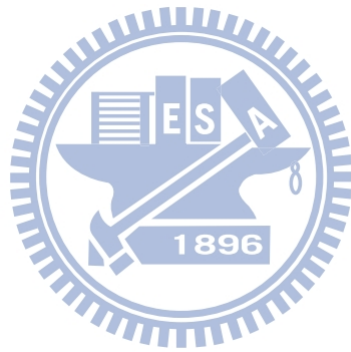


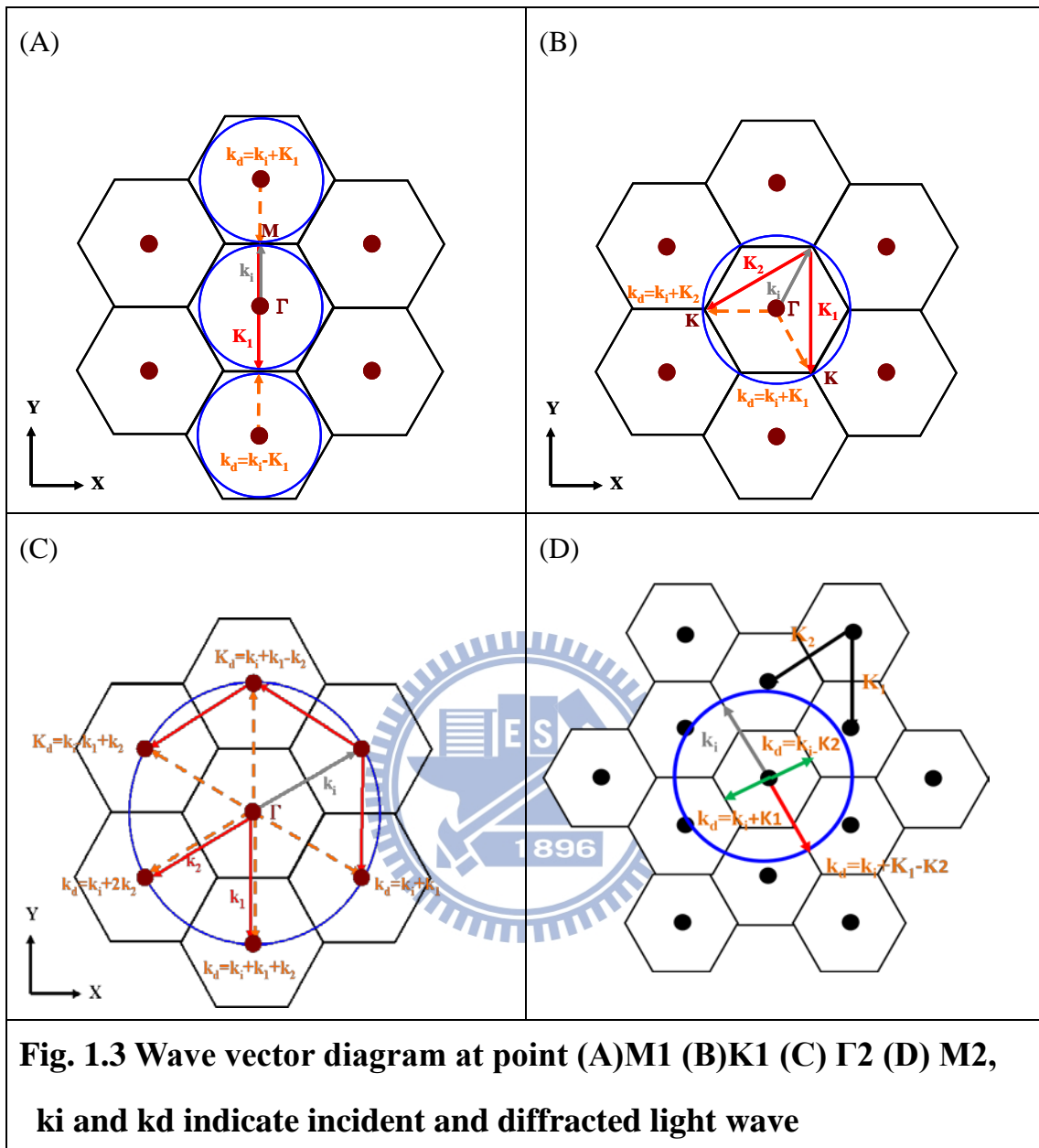
Fig 1.2 (a) The different band edges of triangular lattice photonic crystal in the band diagram (b) Schematic diagram of reciprocal space

the frequency of diffracted light wave, and ω_i is the frequency of incident light wave. Eq. (1.1) represents the phase-matching condition (or momentum conservation), and Eq. (1.2) represents the constant-frequency condition (or energy conservation). When both of equations are satisfied, the lasing behavior would be observed.

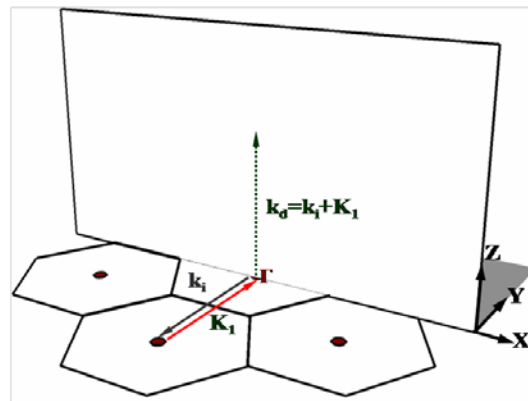
It is expected lasing occurs at specific points on the Brillouin-zone boundary (Γ , M, and K) and at the points at which bands cross and split. At these lasing points, waves propagating in different directions couple to significantly increase the mode density. It is particularly interesting that each of these points exhibits a different type of wave coupling. For example, as shown in Fig. 1.3(a), the coupling at point M1 only involves two waves, propagating in the forward and backward directions. This coupling is similar to that of a conventional DFB laser. However, there can be six equivalent Γ -M directions in the structure; that is, the cavity can exist independently in each of the three different directions to form three independent lasers. Point K1 has a unique coupling characteristic unachievable in conventional DFB lasers, the coupling of waves propagating in three different directions as shown in Fig. 1.2(b). This means the cavity is a triangular. In fact, there can also be six Γ -K directions in the structure; therefore, two different lasing cavities in different Γ -K directions coexist independently. At point Γ the coupling includes waves in in-plane all six directions; 0° , 60° , 120° , -60° , -120° , and 180° as shown in Fig. 1.2(c). In addition, the coupled light can be emitted perpendicular from the surface according to first order Bragg diffraction, as shown in Fig. 1.3(a). This is the same phenomenon that occurs in conventional grating-coupled surface-emitting lasers. The light wave of band-edges M2, K2 and M3 are also diffraction to an oblique direction vertically. For example, Fig. 1.3(b) shows the wave-vector diagram of K2 point where the light wave

is diffracted to an angle tilt 30° normally from the sample surface. Fig. 1.3(c) the wave-vector diagram of one M' point where the light wave is diffracted into three independent angles tilted of about 22.3° and 51° normally from the sample surface, respectively. In these studies, we focus on the folded Γ_2 point because of the 90° normally light wave from the sample surface

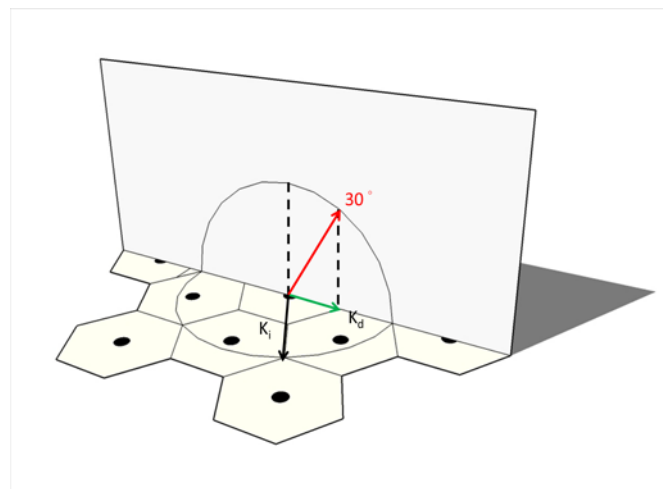




(a)



(b)



(c)

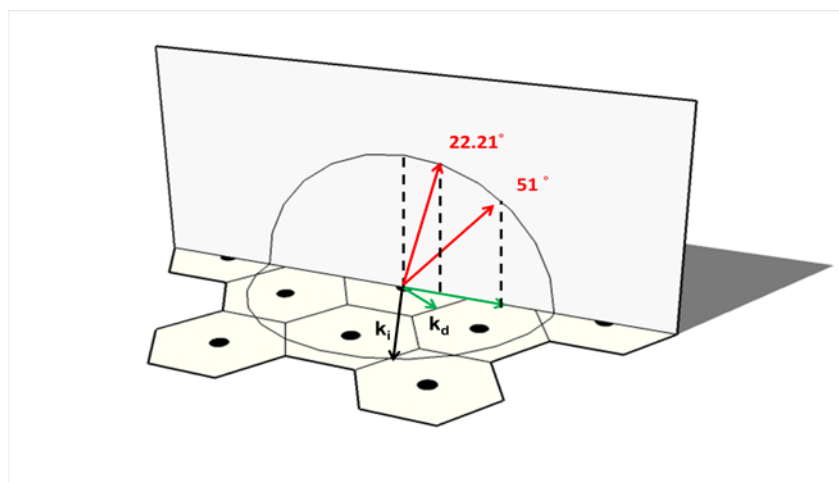


Fig. 1.4 The wave vector diagram at point Γ , K_2 , M_3 in vertical direction

1.3 Outline of the thesis

This thesis has been organized in the following arrangement. The first chapter of the thesis will introduce the different types of edge emission and surface emission lasers and the theory of Bragg diffraction in 2D photonic crystal. Chapter 2 begins by laying out the theoretical dimensions of the research, the couple wave theory and the finite difference method for square lattice and triangular lattice. Chapter 3 describes the simulation results, characteristics and calculated result of PCSEs. The last chapter assesses the conclusion and future work.



References

- [1] A. L. Schawlow and C. H. Townes, *Phys. Rev.* **112**, 1940 (1958)
- [2] T. H. Maiman, *Nature* **187**, 493 (1960)
- [3] R. N. Hall, G. E. Fenner, J. D. Kingsley, T. J. Soltys, *Phys. Rev. Lett.* **9**, 366 (1962)
- [4] N. Holonyak Jr. and S. F. Bevacqua, *Appl. Phys. Lett.* **1**, 82 (1962)
- [5] T. M. Quist, R. H. Rediker, R. J. Keyes, W. E. Krag Lax, A. L. McWhorter, H. J. Zeigler, *Appl. Phys. Lett.* **1**, 91 (1962)
- [6] 盧廷昌、王興宗，「半導體雷射導論」，五南出版社，2008
- [7] M. Meier, A. Mekis, A. Dodabalapur, A. Timko, R. E. Slusher, J. D. Joannopoulos, and O. Nalamasu, *Appl. Phys. Lett.* **74**, 7 (1999)
- [8] M. Imada, A. Chutinan, S. Noda and M. Mochizuki, *Phys. Rev. B.* **65**, 195306 (2002)
- [9] I. Vurgaftman and J. Meyer, *IEEE J. Quantum. Electronics.* **39**, 689 (2003)
- [10] Ohnishi, D., Okano, T., Imada, M. and Noda, S, *Opt. Express.* **12**, 1562 (2004)
- [11] Kim, M, C. S. Kim, W. W. Bewley, J. R. Lindle, C. L. Canedy, I. Vurgaftman and J. R. Meyer, *Appl. Phys. Lett.* **88**, 191105 (2006)
- [12] H. Matsubara, S Yoshimoto, H. Saito, Y. Jianglin, Y. Tanaka and S. Noda, *Science.* **319**, 445 (2008)
- [13] T. C. Lu, S. W. Chen, L. F. Lin, T. T. Kao, C. C. Kao, P. Yu, H. C. Kuo, S. C. Wang and S. H. Fan, *Appl. Phys. Lett.* **92**, 011129 (2008)
- [14] K. Sakoda, K. Ohtaka and T. Ueta, *Opt. Express.* **4**, 481 (1999)
- [15] Y. H. Lee, H. Y. Ryu and M. Notomi, *Phys. Rev. B.* **68**, 045209 (2003)
- [16] K. Sakai, J. Yue and S. Noda, *Opt. Express.* **16**, 6033 (2008)
- [17] K. Sakai, E. Miyai and S. Noda, *IEEE J. Quantum Electron.* **46**, 788 (2010)

[18] S. Nojima, J. Appl. Phys. **98**, 043102 (2005)

[19] M. Notomi, H. Suzuki, and T. Tamamura, Appl. Phys. Lett., **78**, 1325 (2001)



Chapter 2

Fundamentals of Photonic Crystal Surface Emitting Lasers

Introduction

Electromagnetic can be divided into two classes by the direction of polarization : transverse electric (TE) polarized light and transverse magnetic (TM) polarized light, as shown in Fig. 2.1. The light's electromagnetic properties are defined by the orientation of its electric and magnetic fields. TE polarized light is characterized by its magnetic field being parallel to the orientation of photonic crystal columns and hence the electric field is perpendicular to the orientation of photonic crystal columns. And TM polarized light is characterized by its electric field being parallel to the orientation of photonic crystal columns. Here we mainly discuss the TE wave in the photonic crystal.

Square lattice photonic crystal and triangular lattice photonic crystal are common two-dimensional (2D) photonic crystal. So we discuss the Square lattice photonic crystal and triangular lattice photonic crystal, respectively.

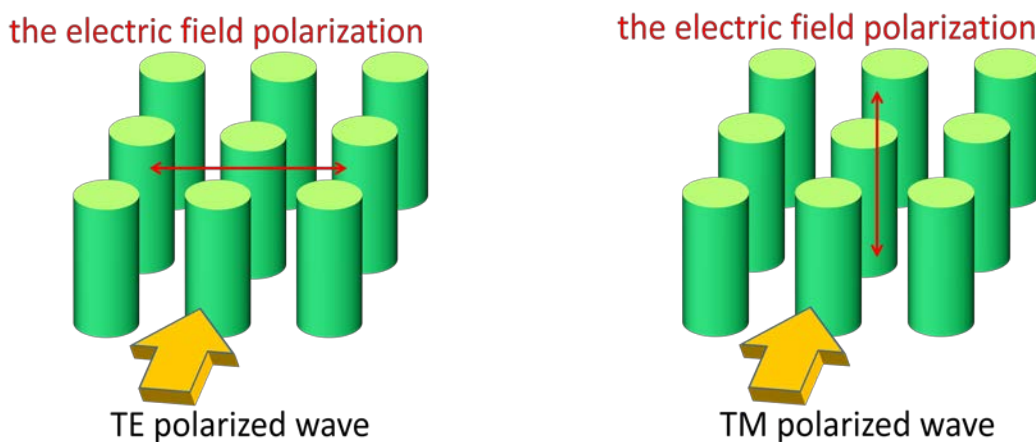


Fig. 2.1 Schematic diagram of the polarization direction of wave

2.1.1 Couple-wave theory for square lattice [1-3]

We first consider the photonic crystal (PC) structure of a square lattice. The PC of circular holes with period a is in the $x-y$ plane, as shown in Fig. 2.2(a). The structure is assumed to be uniform in the z direction. The dielectric constants of the circular holes is ϵ_a and the background material is ϵ_b . The circular holes form a 2D Bravais lattice with sites given by the vectors :

$$r(t) = n_1 \hat{a}_1 + n_2 \hat{a}_2. \quad (2.1)$$

Here, \hat{a}_1 and \hat{a}_2 are the two primitive basis translation vectors of the square lattice. n_1 and n_2 are any integer numbers. The enclosed area of the primitive unit cell of the lattice is $A_c = |a_1 \times a_2| = a^2$.

The vectors $G(m)$ of reciprocal lattice which is shown as Fig. 2.2(b) are given by :

$$G(m) = m_1 \hat{b}_1 + m_2 \hat{b}_2. \quad (2.2)$$

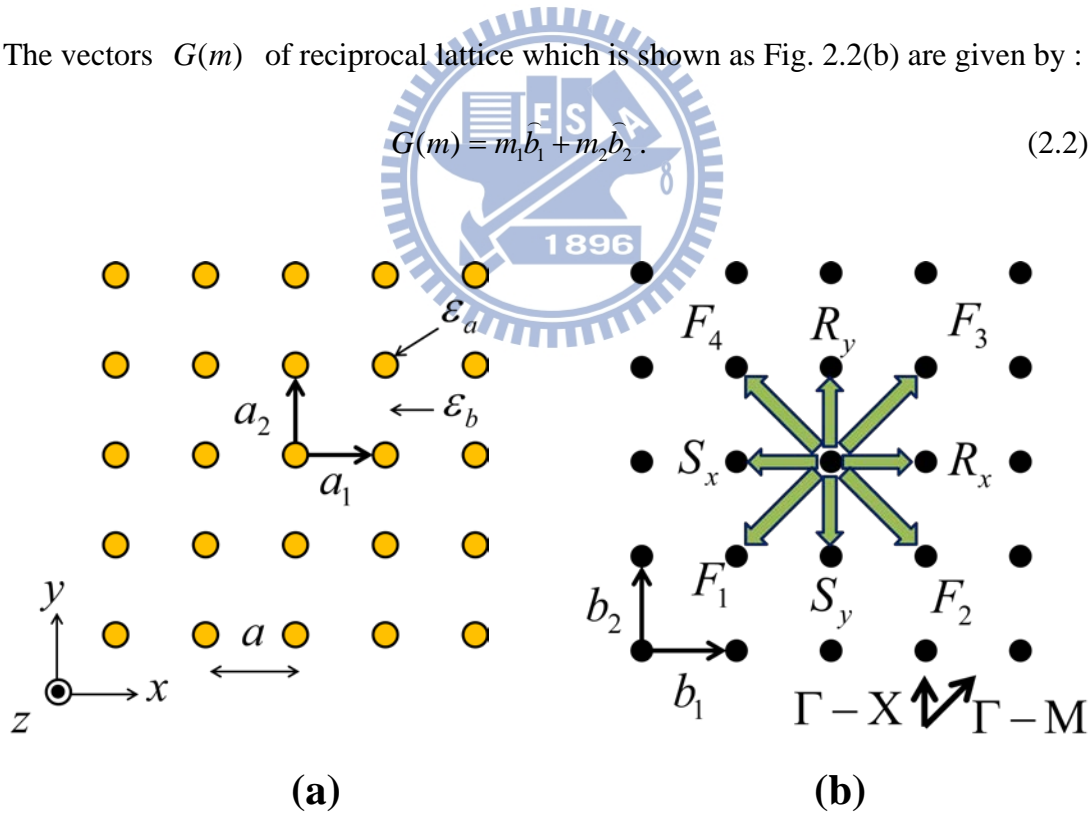


Fig. 2.2 (a) Square lattice photonic crystal structure (b) Schematic diagram of eight propagation waves in square reciprocal lattice photonic crystal structure

Here, \hat{b}_1 and \hat{b}_2 are the two primitive basis translation vectors of this reciprocal lattice. m_1 and m_2 are any integer numbers. The definition of the primitive lattice vectors changes the reciprocal lattice vectors satisfies that

$$\hat{a}_i \cdot \hat{b}_j = 2\pi\delta_{ij} \quad i, j = 1, 2. \quad (2.3)$$

δ_{ij} is delta function and the definition is

$$\delta_{ij} = \begin{cases} 1, & \text{if } i = j \\ 0, & \text{if } i \neq j \end{cases} \quad (2.4)$$

So the two primitive basis translation vectors of this reciprocal lattice are given by

$$\begin{aligned} \hat{b}_1 &= \frac{2\pi}{A_c} (\hat{a}_{2y}, -\hat{a}_{2x}) \\ \hat{b}_2 &= \frac{2\pi}{A_c} (-\hat{a}_{1y}, \hat{a}_{1x}) \end{aligned} \quad (2.5)$$

Where \hat{a}_{ij} is the j_{th} Cartesian component, x or y , of \hat{a}_i ($i=1$ or 2). If we express the primitive translation vectors as $\hat{a}_1 = (a, 0)$ and $\hat{a}_2 = (0, a)$, as shown in Fig. 2.2(a), the primitive reciprocal lattice vectors are $\hat{b}_1 = (2\pi/a, 0)$ and $\hat{b}_2 = (0, 2\pi/a)$, as shown in Fig. 2.2(b). At first, we would need to find the special wave vectors that have contributions at those points of Γ_2 .

The scalar wave equation for the magnetic field H_z in the TE polarization mode can be written as the form [4] :

$$\frac{\partial}{\partial x} \left(\frac{1}{k^2} \frac{\partial H_z}{\partial x} \right) + \frac{\partial}{\partial y} \left(\frac{1}{k^2} \frac{\partial H_z}{\partial y} \right) + H_z = 0 \quad (2.6)$$

where the constant k is given by [5] :

$$k^2 = \left(\frac{2\pi}{\lambda} \right)^2 \sum_G \varepsilon_G e^{iG \cdot r} + i \frac{2\pi \sqrt{\varepsilon_0}}{\lambda} \sum_G \alpha_G e^{iG \cdot r} \quad (2.7)$$

We note that the sign of the second term was negative [5]. In the above formula, λ is the wavelength of the light in free space, ε_G is the Fourier coefficient of the

modulated dielectric constant $\varepsilon(r)$, $\varepsilon_0 (= \varepsilon_{G=0})$ is the averaged dielectric constant, and α_G is the Fourier coefficient of the modulated gain constant $\alpha(r)$. In the Eq.

(2.7), we set that

$$\alpha \ll \beta \equiv \frac{2\pi\sqrt{\varepsilon_0}}{\lambda}, \alpha_G \ll \beta, \varepsilon_{G \neq 0} \ll \varepsilon_0. \quad (2.8)$$

These settings allow us to express the constant k as the form :

$$\frac{1}{k^2} = \frac{1}{\beta^4} \left(\beta^2 - i2\alpha\beta + 2\beta \sum_{G \neq 0} \kappa_G e^{iG \cdot r} \right). \quad (2.9)$$

Here, $\alpha \left(= \frac{\alpha_{G=0}}{2} \right)$ is the averaged gain constant and κ_G is the coupling constant

which can be expressed as :

$$\kappa_G = -\frac{\pi}{\lambda\sqrt{\varepsilon_0}} \varepsilon_G - i \frac{\alpha_G}{2} \quad (2.10)$$

In Eq. (2.9), the periodic variation in the refractive index is included the small perturbation in third term through the Fourier expansion. In the Fourier expansion, the periodic perturbation terms generates an infinite set of diffraction orders. However, as the cavity mode frequency is sufficient close to the Bragg frequency, only the second order diffraction and below can do significant contribution, others can consider to be neglected. We consider the resonance at Γ -point, in which when it is satisfy the second order Bragg diffraction, it will induce 2D optical coupling and result in surface emission. The corresponding coupling coefficient constant κ_i ($i=1, 2, 3$) are denoted as :

$$\begin{aligned} \kappa_1 &= \kappa_G \Big|_{|G|=\beta_0} \\ \kappa_2 &= \kappa_G \Big|_{|G|=\sqrt{2}\beta_0} \\ \kappa_3 &= \kappa_G \Big|_{|G|=2\beta_0} \end{aligned} \quad (2.11)$$

where $\beta_0 = \frac{2\pi}{a}$. Fig. 2.3 shows a schematic illustration of the pairs of wave vectors

that are coupled in each of these three cases. Coupling constant κ_1 describes the intensity of the coupling of two plane waves propagating at 45° to each other. Coupling constant κ_2 describes the intensity of the coupling of two plane waves propagating in directions perpendicular to each other. Coupling constant κ_3 describes the intensity of the coupling of counterpropagating waves to each other, which corresponds to the backward scattering in second-order distributed feedback (DFB) lasers. The coupling constant κ_2 does not exist in the case of a square lattice with TE polarization. This is because the electric fields of two waves propagating in perpendicular directions are orthogonal to each other and the overlap integral vanishes.

While considering a periodic structure, the magnetic field can be described by the Bloch mode [4] :

$$H_z(r) = \sum_G H_G e^{-i(k+G)r} \quad (2.12)$$

H_G is the amplitude of each plane wave, k is the wave vector in the first Brillouin zone and when it is the Γ point, it comes to zero. However, at the specific Γ point

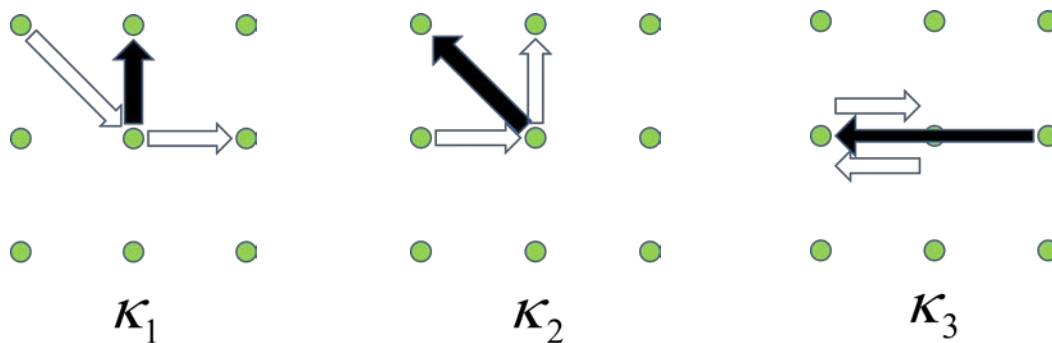


Fig. 2.3 Diffraction diagram for each coupling constant for square lattice. White arrows indicate pairs of wave vectors and black arrows indicate the corresponding reciprocal lattice vectors.

discussed for 2D photonic crystal, there are eight propagating waves in PC structure denoted as $R_x, S_x, R_y, S_y, F_1, F_2, F_3, F_4$ showed in Fig. 2.2(b), the first four items are the complex amplitudes of the four propagating waves along the $x, -x, y, -y$ directions and the other four items are the complex amplitudes of the four propagating waves along $\Gamma - M$ directions, respectively. Those correspond to H_G in Eq. (2.12). Here, we do consider these basic wave vectors along the $\Gamma - X$ directions with $|\kappa + G| = \beta_0$ and $\Gamma - M$ directions with $|\kappa + G| = \sqrt{2}\beta_0$ [1]. The contribution of the higher order waves with $|\kappa + G| \geq 2\beta_0$, are considered to be negligible. We should note that the basic waves and higher order waves are partial waves of the Bloch mode, so they have the same eigenvalue β for specific resonant cavity mode.

Using these eight waves, the magnetic field in this case can be rewritten the expression as the following sum :

$$H_z(r) = R_x(x, y)e^{-i\beta_0 x} + S_x(x, y)e^{i\beta_0 x} + R_y(x, y)e^{-i\beta_0 y} + S_y(x, y)e^{-i\beta_0 y} + F_1 e^{i\beta_0 x + i\beta_0 y} + F_2 e^{-i\beta_0 x + i\beta_0 y} + F_3 e^{i\beta_0 x - i\beta_0 y} + F_4 e^{-i\beta_0 x - i\beta_0 y} \quad (2.13)$$

By substituting Eq. (2.9) and Eq. (2.13) into Eq. (2.6), then using Eq. (2.11) and comparing the exponential terms, we obtain eight equations of the form :

$$-\frac{\partial}{\partial x} R_x + (\alpha - i\delta)R_x = i\kappa_3 S_x - i\kappa_1 F_2 - i\kappa_1 F_4 \quad (2.14a)$$

$$\frac{\partial}{\partial x} S_x + (\alpha - i\delta)S_x = i\kappa_3 R_x - i\kappa_1 F_1 - i\kappa_1 F_3 \quad (2.14b)$$

$$-\frac{\partial}{\partial y} R_y + (\alpha - i\delta)R_y = i\kappa_3 S_y - i\kappa_1 F_3 - i\kappa_1 F_4 \quad (2.14c)$$

$$\frac{\partial}{\partial y} S_y + (\alpha - i\delta)S_y = i\kappa_3 R_y - i\kappa_1 F_1 - i\kappa_1 F_2 \quad (2.14d)$$

$$\frac{\partial}{\partial x} F_1 + \frac{\partial}{\partial y} F_1 + (2\alpha - i\delta)F_1 + i\frac{\beta_0}{2} F_1 = -i\kappa_1 S_x - i\kappa_1 S_y \quad (2.14e)$$

$$-\frac{\partial}{\partial x} F_2 + \frac{\partial}{\partial y} F_2 + (2\alpha - i\delta)F_2 + i\frac{\beta_0}{2} F_2 = -i\kappa_1 R_x - i\kappa_1 S_y \quad (2.14f)$$

$$\frac{\partial}{\partial x} F_3 - \frac{\partial}{\partial y} F_3 + (2\alpha - i\delta)F_3 + i\frac{\beta_0}{2}F_3 = -i\kappa_1 S_x - i\kappa_1 R_y \quad (2.14g)$$

$$-\frac{\partial}{\partial x} F_4 - \frac{\partial}{\partial y} F_4 + (2\alpha - i\delta)F_4 + i\frac{\beta_0}{2}F_4 = -i\kappa_1 R_x - i\kappa_1 R_y \quad (2.14h)$$

The parameter δ is a normalized frequency defined by

$$\delta \equiv \frac{\beta^2 - \beta_0^2}{2\beta_0} \approx \beta - \beta_0 = \frac{n}{c}(\omega - \omega_0) \quad (2.15)$$

where n is the averaged refractive index, which is equal to $\sqrt{\varepsilon_0}$ and c is the speed of light in free space. The parameter δ is a measure of the deviation of the oscillation frequency ω from the Bragg frequency ω_0 . In the above equations, we assume that $\beta/\beta_0 \approx 1$, since we take optical coupling at Γ point and this frequency deviation is small.

One thing we should noted that the coupling coefficient κ_2 , which describes the intensity of the direct coupling of waves propagating perpendicular to each other along the x and y axes, does not exist in Eq. (2.14) [1]. We can neglect both the first two derivatives and the third terms in each case on the left hand side of Eq. (2.14e)~Eq. (2.14h), because the amplitudes vary only slowly and $\alpha, \delta \ll \beta_0$ for the lower-order resonant modes. Then by substituting Eq. (2.14e)~Eq. (2.14h) into Eq. (2.14a)~Eq. (2.14d) and including diffraction in the direction vertical to the PC plane represented by the coupling constant κ_0 [6][7], we obtain four equations of the form :

$$(\alpha - \kappa_0 - i\delta)R_x - \frac{\partial}{\partial x} R_x = i\frac{4\kappa_1^2}{\beta_0} R_x + (i\kappa_3 - \kappa_0)S_x + i\frac{2\kappa_1^2}{\beta_0} S_y + i\frac{2\kappa_1^2}{\beta_0} R_y \quad (2.16a)$$

$$(\alpha - \kappa_0 - i\delta)S_x + \frac{\partial}{\partial x} S_x = i\frac{4\kappa_1^2}{\beta_0} S_x + (i\kappa_3 - \kappa_0)R_x + i\frac{2\kappa_1^2}{\beta_0} S_y + i\frac{2\kappa_1^2}{\beta_0} R_y \quad (2.16b)$$

$$(\alpha - \kappa_0 - i\delta)R_y - \frac{\partial}{\partial y} R_y = i\frac{4\kappa_1^2}{\beta_0} R_y + (i\kappa_3 - \kappa_0)S_y + i\frac{2\kappa_1^2}{\beta_0} S_x + i\frac{2\kappa_1^2}{\beta_0} R_x \quad (2.16c)$$

$$(\alpha - \kappa_0 - i\delta)S_y + \frac{\partial}{\partial y}S_y = i\frac{4\kappa_1^2}{\beta_0}S_y + (i\kappa_3 - \kappa_0)R_y + i\frac{2\kappa_1^2}{\beta_0}S_x + i\frac{2\kappa_1^2}{\beta_0}R_x \quad (2.16d)$$

For the resonant mode in a square lattice PC cavity with TE polarization, the eigenvalues α provide the threshold gain and the eigenvalues δ provide the frequency deviation from the Bragg condition by numerically solving the Eq. (2.16) under some boundary conditions. The wave on the equal sign of the left in the Eq. (2.16) is meaning that electromagnetic waves in a square lattice PC by moving receive the gain and loss. The wave on the equal sign of the right in the Eq. (2.16) is meaning that electromagnetic waves in a square lattice PC are coupling with R_x, S_x, R_y, S_y , respectively.

The coupling constants for the circular holes are calculated with the formulas [6] :

$$\kappa_G = \left[-\frac{\pi}{a\varepsilon_0}(\varepsilon_a - \varepsilon_b) - i\frac{1}{2}(\alpha_a - \alpha_b) \right] \frac{2f J_1(|G|R)}{|G|R} \quad (2.17)$$

$$\kappa_0 = \frac{d_g}{\Gamma_g} \left| \frac{2\pi\Delta n}{\lambda} \frac{1}{a_L} \iint \exp(-iG_L \cdot r) dx dy \right|^2 \quad (2.18)$$

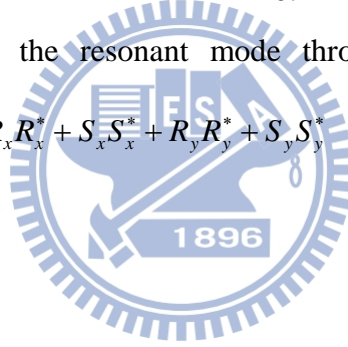
Here, ε_a and ε_b are the dielectric constants and α_a and α_b are the gain constants of the circular holes and the background material, respectively. The quantity $f = \pi R^2 / a^2$ is a hole filling factor and R is the radius of the circular hole. The averaged dielectric constant ε_0 is given by $\varepsilon_0 = \sqrt{\varepsilon_a f + \varepsilon_b(1-f)}$. $J_1(x)$ is a Bessel function of the first kind for integer order one. d_g is the thickness of the grating layer and Γ_g is its confinement factor. Δn is the modulation of the real part of the modal index between the waveguide and the bottom of the etched features with perfectly vertical sidewalls. λ is the grating's resonance wavelength and a_L is the

area of the reciprocal lattice primitive cell. We exclusively define the vertical coupling constant κ_0 using the relation $\kappa_0 L = 2\kappa_1^2 L^2 / 500$, where L is the length of the PC cavity.

We assume the boundary conditions of zero reflectivity and zero gain perturbation $(\alpha_a - \alpha_b)$ in this work. We used the finite difference method as described in the CH2.1.2 for solving the Eq. (2.16). The electric field distribution $E(r, t) = (E_x e^{i\omega t}, E_y e^{i\omega t}, 0)$ is calculated using the time-dependent magnetic field $H(r, t) = (0, 0, H_z e^{i\omega t})$ and Maxwell's equation

$$\nabla \times H(r, t) = \varepsilon(r) \frac{\partial E(r, t)}{\partial t}. \quad (2.19)$$

The intensity envelope of the resonant mode throughout the PC structure is determined using the sum $R_x R_x^* + S_x S_x^* + R_y R_y^* + S_y S_y^*$



2.1.2 Finite difference method for square lattice

We discuss the main relationship of the threshold gain α and the frequency deviation δ from the Bragg condition. And Eq. (2.16) are the eigenvalue problems.

So, we change the Eq. (2.16) to the following form :

$$(\alpha - \kappa_0 - i\delta)R_x = \left(\frac{\partial}{\partial x} + i\frac{4\kappa_1^2}{\beta_0}\right)R_x + (i\kappa_3 - \kappa_0)S_x + i\frac{2\kappa_1^2}{\beta_0}S_y + i\frac{2\kappa_1^2}{\beta_0}R_y \quad (2.20a)$$

$$(\alpha - \kappa_0 - i\delta)S_x = \left(-\frac{\partial}{\partial x} + i\frac{4\kappa_1^2}{\beta_0}\right)S_x + (i\kappa_3 - \kappa_0)R_x + i\frac{2\kappa_1^2}{\beta_0}S_y + i\frac{2\kappa_1^2}{\beta_0}R_y \quad (2.20b)$$

$$(\alpha - \kappa_0 - i\delta)R_y = \left(\frac{\partial}{\partial y} + i\frac{4\kappa_1^2}{\beta_0}\right)R_y + (i\kappa_3 - \kappa_0)S_y + i\frac{2\kappa_1^2}{\beta_0}S_x + i\frac{2\kappa_1^2}{\beta_0}R_x \quad (2.20c)$$

$$(\alpha - \kappa_0 - i\delta)S_y = \left(-\frac{\partial}{\partial y} + i\frac{4\kappa_1^2}{\beta_0}\right)S_y + (i\kappa_3 - \kappa_0)R_y + i\frac{2\kappa_1^2}{\beta_0}S_x + i\frac{2\kappa_1^2}{\beta_0}R_x \quad (2.20d)$$

Now we can make the matrix of Eq. (2.20), as the following form :

$$(\alpha - \kappa_0 - i\delta) \begin{bmatrix} R_x \\ S_x \\ R_y \\ S_y \end{bmatrix} = \begin{bmatrix} A + \frac{\partial}{\partial x} & B & C & C \\ B & A - \frac{\partial}{\partial x} & C & C \\ C & C & A + \frac{\partial}{\partial y} & B \\ C & C & B & A - \frac{\partial}{\partial y} \end{bmatrix} \begin{bmatrix} R_x \\ S_x \\ R_y \\ S_y \end{bmatrix} \quad (2.21)$$

Here, $A = i\frac{4\kappa_1^2}{\beta_0}$, $B = i\kappa_3 - \kappa_0$, $C = i\frac{2\kappa_1^2}{\beta_0}$. There is a differential item in the matrix.

The differential item is complex and difficult in the matrix operations. The finite difference method that difference is used in place of differential can simplify the problems. Numerical solution of the coupled wave Eq. (2.21) can be found by using the finite difference method. There are several hundred or thousand of the photonic crystal in the x and y directions of the practical devices. However, we cut apart this photonic crystal cavity into a 18×18 matrix for the calculations, as shown in Fig. 2.4. We solve the Eq. (2.21) and get the numerical solution that is the complex amplitudes at each positions by black dots. The value of each white dot can obtain by using the complex amplitudes of the neighboring black dots. For example, the

difference equation corresponding to Eq. (2.20a) is written in the form :

$$\begin{aligned}
& (\alpha - \kappa_0 - i\delta) \frac{R_x(j, k) + R_x(j+1, k)}{2} \\
&= \frac{R_x(j+1, k) - R_x(j, k)}{d} + i \frac{4\kappa_1^2}{\beta_0} \frac{R_x(j, k) + R_x(j+1, k)}{2} \\
&+ (i\kappa_3 - \kappa_0) \frac{S_x(j, k) + S_x(j+1, k)}{2} \\
&+ i \frac{2\kappa_1^2}{\beta_0} \frac{S_y(j, k) + S_y(j, k+1)}{2} + i \frac{2\kappa_1^2}{\beta_0} \frac{R_y(j, k) + R_y(j, k+1)}{2}
\end{aligned} \tag{2.22}$$

where d is the side length of one segment, and j and k denote the index along the x and y directions, respectively. At all the surrounding boundaries, we set the facet reflection to zero :

$$R_x(-\frac{L}{2}, y) = S_x(\frac{L}{2}, y) = R_y(x, -\frac{L}{2}) = S_y(x, \frac{L}{2}) = 0 \tag{2.23}$$

where L is the length of a square photonic crystal cavity. By solving the eigenvalue problem for the sets of difference equations, we obtain the eigenvalue $(\alpha - \kappa_0 - i\delta)$ and the eigenvectors $(R_x(j, k), S_x(j, k), R_y(j, k), S_y(j, k), etc)$.

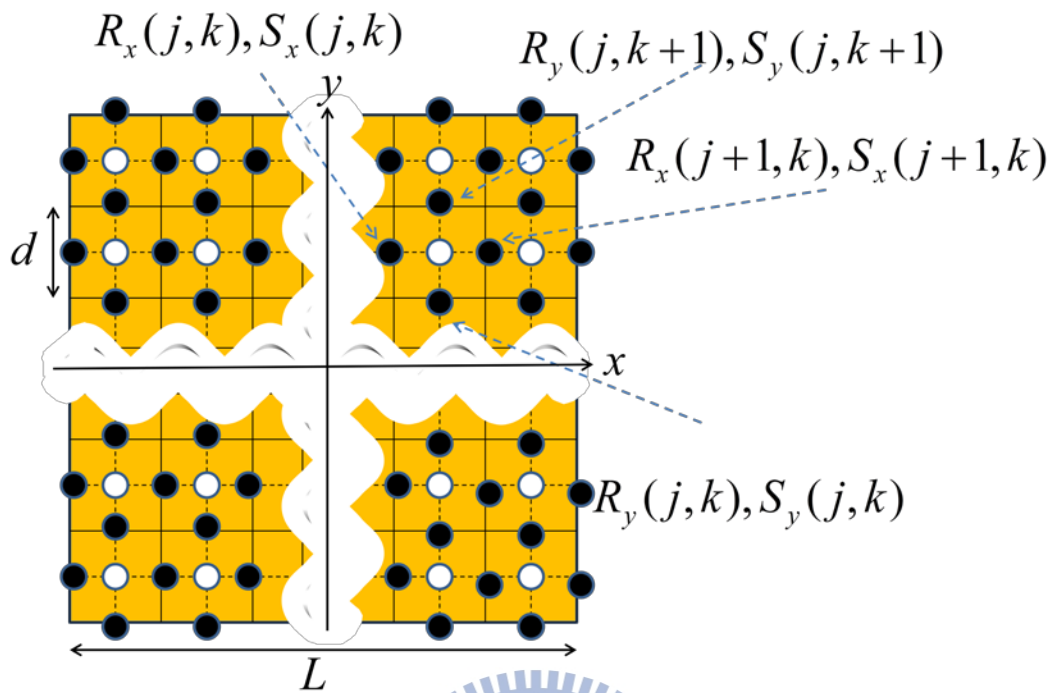


Fig. 2.4 Schematic diagram for square lattice for the finite difference method. The target of calculations is carried out at the positions of the white dots by using the complex amplitudes of the neighboring black dots.

2.2.1 Couple-wave theory for triangular lattice

In this section, we consider the PC structure for triangular lattice. The 2D PC structure investigated here consists of a triangular lattice with circular holes with period a in the $x-y$ plane, as shown in Fig. 2.5(a). The structure is assumed to be uniform in the z direction. The dielectric constants of the circular holes is ϵ_a and the background material is ϵ_b . The enclosed area of the primitive unit cell of the lattice for triangular lattice is $A_c = |a_1 \times a_2| = \frac{\sqrt{3}a^2}{2}$. If we express the primitive translation vectors as $\hat{a}_1 = \left(\frac{\sqrt{3}a}{2}, \frac{a}{2} \right)$ and $\hat{a}_2 = (0, a)$, as shown in Fig. 2.5(a), the primitive reciprocal lattice vectors are $\hat{b}_1 = \left(\frac{4\pi}{\sqrt{3}a}, 0 \right)$ and $\hat{b}_2 = \left(\frac{-2\pi}{\sqrt{3}a}, \frac{2\pi}{a} \right)$, as shown in Fig. 2.5(b).

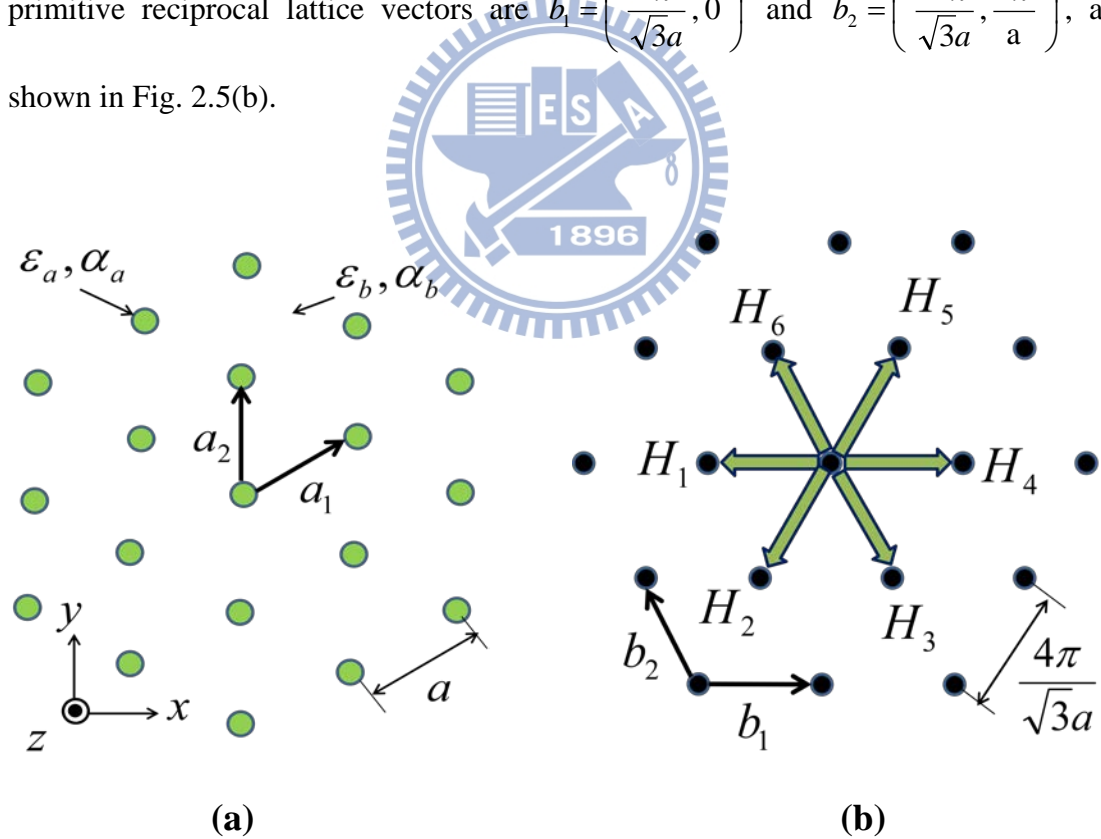


Fig 2.5 (a) Triangular lattice photonic crystal structure (b) Schematic diagram of six propagation waves in triangular reciprocal lattice photonic crystal structure

The scalar wave equation for the magnetic field H_z in the TE polarization mode can be written as the form [4] :

$$\frac{\partial}{\partial x} \left(\frac{1}{k^2} \frac{\partial H_z}{\partial x} \right) + \frac{\partial}{\partial y} \left(\frac{1}{k^2} \frac{\partial H_z}{\partial y} \right) + H_z = 0 \quad (2.24)$$

where the constant k is given by [5] :

$$k^2 = \left(\frac{2\pi}{\lambda} \right)^2 \sum_G \varepsilon_G e^{iG \cdot r} + i \frac{2\pi \sqrt{\varepsilon_0}}{\lambda} \sum_G \alpha_G e^{iG \cdot r} \quad (2.25)$$

Here, λ is the wavelength of the light in free space, ε_G is the Fourier coefficient of the modulated dielectric constant $\varepsilon(r)$, $\varepsilon_0 (= \varepsilon_{G=0})$ is the averaged dielectric constant, and α_G is the Fourier coefficient of the modulated gain constant $\alpha(r)$. In the Eq. (2.25), we set low perturbation that

$$\alpha \ll \beta \equiv \frac{2\pi \sqrt{\varepsilon_0}}{\lambda}, \alpha_G \ll \beta, \varepsilon_{G \neq 0} \ll \varepsilon_0. \quad (2.26)$$

These settings allow us to express the constant k as the form :

$$\frac{1}{k^2} = \frac{1}{\beta^4} \left(\beta^2 - i2\alpha\beta + 2\beta \sum_{G \neq 0} \kappa_G e^{iG \cdot r} \right). \quad (2.27)$$

Here, $\alpha \left(= \frac{\alpha_{G=0}}{2} \right)$ is the averaged gain constant and κ_G is the coupling constant which can be expressed as :

$$\kappa_G = -\frac{\pi}{\lambda \sqrt{\varepsilon_0}} \varepsilon_G - i \frac{\alpha_G}{2} \quad (2.28)$$

We consider the resonance at Γ -point, in which when it is satisfy the second order Bragg diffraction, it will induce 2D optical coupling and result in surface emission.

The corresponding coupling coefficient constant κ_i ($i = 1, 2, 3$) are denoted as :

$$\begin{aligned} \kappa_1 &= \kappa_G \Big|_{|G|=\beta_0} \\ \kappa_2 &= \kappa_G \Big|_{|G|=\sqrt{3}\beta_0} \\ \kappa_3 &= \kappa_G \Big|_{|G|=2\beta_0} \end{aligned} \quad (2.29)$$

where $\beta_0 = \frac{4\pi}{\sqrt{3}a}$. Fig. 2.6 shows a schematic illustration of the pairs of wave vectors that are coupled in each of these three cases. Coupling constant κ_1 describes the intensity of the coupling of two plane waves propagating at 60° to each other. Coupling constant κ_2 describes the intensity of the coupling of two plane waves propagating at 120° to each other. Coupling constant κ_3 describes the intensity of the coupling of counterpropagating waves to each other, which corresponds to the backward scattering in second-order distributed feedback (DFB) lasers.

While considering periodic structure, the magnetic field can be described by the Bloch mode [4]

$$H_z(r) = \sum_G H_G e^{-i(k+G)r} \quad (2.30)$$

H_G is the amplitude of each plane wave, k is the wave vector in the first Brillouin zone and when it is the Γ point, it comes to zero. However, at the specific Γ point discussed in this case, the amplitude H_G with $|G| = \beta_0$ are significant and the other amplitudes are small and can be neglected. For 2D photonic crystal, there are six propagating waves with $|G| = \beta_0$ in PC structure denoted as $H_1, H_2, H_3, H_4, H_5,$

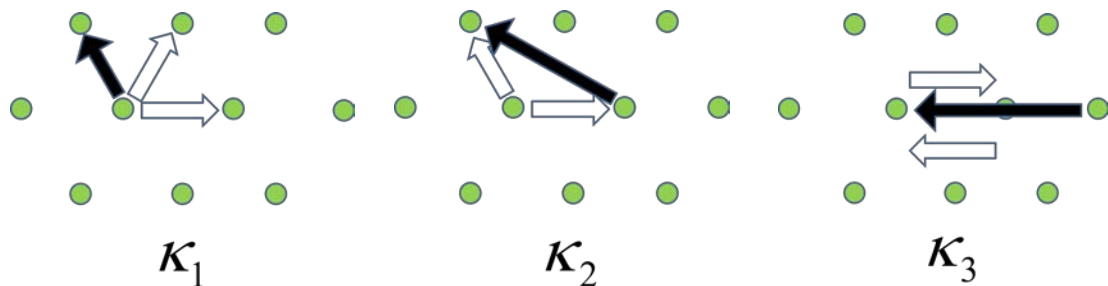


Fig. 2.6 Diffraction diagram for each coupling constant for triangular lattice. White arrows indicate pairs of wave vectors and black arrows indicate the corresponding reciprocal lattice vectors.

H_6 . All of these parameters which are shown in Fig. 2.5(b) are considered in our model.

Using these six waves, the magnetic field in this case can be rewritten the expression as the following sum :

$$H_z(r) = H_1 e^{-i\beta_0 x} + H_2 e^{-i\beta_0 \left(\frac{x}{2} + \frac{\sqrt{3}}{2} y \right)} + H_3 e^{-i\beta_0 \left(\frac{x}{2} + \frac{\sqrt{3}}{2} y \right)} + H_4 e^{i\beta_0 x} + H_5 e^{-i\beta_0 \left(\frac{x}{2} + \frac{\sqrt{3}}{2} y \right)} + H_6 e^{-i\beta_0 \left(\frac{x}{2} + \frac{\sqrt{3}}{2} y \right)}. \quad (2.31)$$

By substituting Eq. (2.27), Eq. (2.28) and Eq. (2.31) into wave Eq. (2.24), then using Eq. (2.29), including diffraction in the direction vertical to the PC plane represented by the coupling constant κ_0 [6][7] and comparing the exponential terms, we obtain six equations of the form :

$$-\frac{\partial}{\partial x} H_1 + (\alpha - \kappa_0 - i\delta) H_1 = -i \frac{\kappa_1}{2} (H_2 + H_6) + i \frac{\kappa_2}{2} (H_3 + H_5) + (i\kappa_3 - \kappa_0) H_4 \quad (2.32a)$$

$$-\frac{1}{2} \frac{\partial}{\partial x} H_2 - \frac{\sqrt{3}}{2} \frac{\partial}{\partial y} H_2 + (\alpha - \kappa_0 - i\delta) H_2 = -i \frac{\kappa_1}{2} (H_1 + H_3) + i \frac{\kappa_2}{2} (H_4 + H_6) + (i\kappa_3 - \kappa_0) H_5 \quad (2.32b)$$

$$\frac{1}{2} \frac{\partial}{\partial x} H_3 - \frac{\sqrt{3}}{2} \frac{\partial}{\partial y} H_3 + (\alpha - \kappa_0 - i\delta) H_3 = -i \frac{\kappa_1}{2} (H_2 + H_4) + i \frac{\kappa_2}{2} (H_1 + H_5) + (i\kappa_3 - \kappa_0) H_6 \quad (2.32c)$$

$$\frac{\partial}{\partial x} H_4 + (\alpha - \kappa_0 - i\delta) H_4 = -i \frac{\kappa_1}{2} (H_3 + H_5) + i \frac{\kappa_2}{2} (H_2 + H_6) + (i\kappa_3 - \kappa_0) H_1 \quad (2.32d)$$

$$\frac{1}{2} \frac{\partial}{\partial x} H_5 + \frac{\sqrt{3}}{2} \frac{\partial}{\partial y} H_5 + (\alpha - \kappa_0 - i\delta) H_5 = -i \frac{\kappa_1}{2} (H_4 + H_6) + i \frac{\kappa_2}{2} (H_1 + H_3) + (i\kappa_3 - \kappa_0) H_2 \quad (2.32e)$$

$$-\frac{1}{2} \frac{\partial}{\partial x} H_6 + \frac{\sqrt{3}}{2} \frac{\partial}{\partial y} H_6 + (\alpha - \kappa_0 - i\delta) H_6 = -i \frac{\kappa_1}{2} (H_1 + H_3) + i \frac{\kappa_2}{2} (H_2 + H_4) + (i\kappa_3 - \kappa_0) H_3 \quad (2.32f)$$

where, H_1, H_2, H_3, H_4, H_5 , and H_6 express the envelope magnetic field distributions of individual light waves propagating in the six equivalent $\Gamma-M$ directions : $0^\circ, +60^\circ, +120^\circ, +180^\circ, +240^\circ$, and $+300^\circ$ with respect to the x axis.

κ_1, κ_2 , and κ_3 are the coupling coefficients between light waves propagating at 60° to each other (H_1 and H_2 , H_2 and H_3 , and so on), at 120° (H_1 and H_3 ,

H_2 , and H_4 , and so on), and at 180° (H_1 and H_4 , H_2 and H_5 , and so on), respectively. δ is the deviation of the wave number β (expressed as $2\pi\omega/c$, where ω is the frequency and c is the velocity of light) from the fundamental propagation constant β_0 (equal to $4\pi/\sqrt{3}a$, where a is the lattice constant) for each cavity mode, and expressed as $\delta = (\beta^2 - \beta_0^2)/2\beta_0$, α is the corresponding threshold gain. For the resonant mode in a triangular lattice PC cavity with TE polarization, the eigenvalues α provide the threshold gain and the eigenvalues δ provide the frequency deviation from the Bragg condition by numerically solving the Eq. (2.32) under some boundary conditions. The wave on the equal sign of the left in the Eq. (2.32) is meaning that electromagnetic waves in a triangular lattice PC by moving receive the gain and loss. The wave on the equal sign of the right in the Eq. (2.32) is meaning that electromagnetic waves in a triangular lattice PC are coupling with H_1, H_2, H_3, H_4, H_5 , and H_6 , respectively.

The coupling constants for the circular holes are calculated with the formulas [6]

$$\kappa_G = \left[-\frac{\pi}{a\varepsilon_0}(\varepsilon_a - \varepsilon_b) - i\frac{1}{2}(\alpha_a - \alpha_b) \right] \frac{2f J_1(|G|R)}{(|G|R)} \quad (2.33)$$

Here, ε_a and ε_b are the dielectric constants and α_a and α_b are the gain constants of the circular holes and the background material, respectively. The quantity $f = \frac{2\pi R^2}{\sqrt{3} a^2}$ is a hole filling factor and R is the radius of the circular hole. The averaged dielectric constant ε_0 is given by $\varepsilon_0 = \varepsilon_a f + \varepsilon_b(1-f)$. $J_1(x)$ is a Bessel function of the first kind for integer order one. The definition of coupling constant κ_0 is the same with that of the square lattice in section 2.1.1.

We assume the boundary conditions of zero reflectivity and zero gain

perturbation $(\alpha_a - \alpha_b)$ in this work. We used the finite difference method as described in the Ch2.2.2 for solving the Eq. (2.32). The electric field distribution $E(r,t) = (E_x e^{i\omega t}, E_y e^{i\omega t}, 0)$ is calculated using the time-dependent magnetic field $H(r,t) = (0, 0, H_z e^{i\omega t})$ and Maxwell's equation

$$\nabla \times H(r,t) = \varepsilon(r) \frac{\partial E(r,t)}{\partial t}. \quad (2.34)$$

The intensity envelope of the resonant mode throughout the PC structure is determined using the sum $H_1 H_1^* + H_2 H_2^* + H_3 H_3^* + H_4 H_4^* + H_5 H_5^* + H_6 H_6^*$



2.2.2 Finite difference method for triangular lattice

We discuss the main relationship of the threshold gain α and the frequency deviation δ from the Bragg condition. And Eq. (2.32) are the eigenvalue problems.

So, we change the Eq. (2.32) to the following form :

$$(\alpha - \kappa_0 - i\delta)H_1 = \frac{\partial}{\partial x}H_1 - i\frac{\kappa_1}{2}(H_2 + H_6) + i\frac{\kappa_2}{2}(H_3 + H_5) + (i\kappa_3 - \kappa_0)H_4 \quad (2.35a)$$

$$(\alpha - \kappa_0 - i\delta)H_2 = \frac{1}{2}\frac{\partial}{\partial x}H_2 + \frac{\sqrt{3}}{2}\frac{\partial}{\partial y}H_2 - i\frac{\kappa_1}{2}(H_1 + H_3) + i\frac{\kappa_2}{2}(H_4 + H_6) + (i\kappa_3 - \kappa_0)H_5 \quad (2.35b)$$

$$(\alpha - \kappa_0 - i\delta)H_3 = -\frac{1}{2}\frac{\partial}{\partial x}H_3 + \frac{\sqrt{3}}{2}\frac{\partial}{\partial y}H_3 - i\frac{\kappa_1}{2}(H_2 + H_4) + i\frac{\kappa_2}{2}(H_1 + H_5) + (i\kappa_3 - \kappa_0)H_6 \quad (2.35c)$$

$$(\alpha - \kappa_0 - i\delta)H_4 = -\frac{\partial}{\partial x}H_4 - i\frac{\kappa_1}{2}(H_3 + H_5) + i\frac{\kappa_2}{2}(H_2 + H_6) + (i\kappa_3 - \kappa_0)H_1 \quad (2.35d)$$

$$(\alpha - \kappa_0 - i\delta)H_5 = -\frac{1}{2}\frac{\partial}{\partial x}H_5 - \frac{\sqrt{3}}{2}\frac{\partial}{\partial y}H_5 - i\frac{\kappa_1}{2}(H_4 + H_6) + i\frac{\kappa_2}{2}(H_1 + H_3) + (i\kappa_3 - \kappa_0)H_2 \quad (2.35e)$$

$$(\alpha - \kappa_0 - i\delta)H_6 = \frac{1}{2}\frac{\partial}{\partial x}H_6 - \frac{\sqrt{3}}{2}\frac{\partial}{\partial y}H_6 - i\frac{\kappa_1}{2}(H_1 + H_5) + i\frac{\kappa_2}{2}(H_2 + H_4) + (i\kappa_3 - \kappa_0)H_3 \quad (2.35f)$$

Now we can make the matrix of Eq. (2.35), as the following form :

$$(\alpha - \kappa_0 - i\delta) \begin{bmatrix} H_1 \\ H_2 \\ H_3 \\ H_4 \\ H_5 \\ H_6 \end{bmatrix} = \begin{bmatrix} \frac{\partial}{\partial x} & A & B & C & B & A \\ A & \frac{\partial}{\partial v_1} & A & B & C & B \\ B & A & \frac{\partial}{\partial v_2} & A & B & C \\ C & B & A & -\frac{\partial}{\partial x} & A & B \\ B & C & B & A & -\frac{\partial}{\partial v_1} & A \\ A & B & C & B & A & -\frac{\partial}{\partial v_2} \end{bmatrix} \begin{bmatrix} H_1 \\ H_2 \\ H_3 \\ H_4 \\ H_5 \\ H_6 \end{bmatrix} \quad (2.36)$$

$$\text{Here, } \frac{\partial}{\partial v_1} = \frac{1}{2}\frac{\partial}{\partial x} + \frac{\sqrt{3}}{2}\frac{\partial}{\partial y}, \quad \frac{\partial}{\partial v_2} = -\frac{1}{2}\frac{\partial}{\partial x} + \frac{\sqrt{3}}{2}\frac{\partial}{\partial y}, \quad A = -i\frac{\kappa_1}{2}, \quad B = i\frac{\kappa_2}{2},$$

$C = i\kappa_3 - \kappa_0$ v_1 and v_2 are the $(\frac{1}{2}, \frac{\sqrt{3}}{2})$ and $(-\frac{1}{2}, \frac{\sqrt{3}}{2})$ of direction vector,

respectively. There is a differential item in the matrix. The differential item is complex and difficult in the matrix operations. The finite difference method that difference is

used in place of differential can simplify the problems. Numerical solution of the coupled wave Eq. (2.36) can be found by using the finite difference method. There are several hundred or thousand of the photonic crystal in the $x-y$ plane of the practical devices. However, we cut apart this photonic crystal cavity into a matrix for the calculations, as shown in Fig. 2.7. We solve the Eq. (2.36) and get the numerical solution that is the complex amplitudes at each positions by black dots. The value of each white dot can obtain by using the complex amplitudes of the neighboring black dots. For example, the difference equation corresponding to Eq. (2.35a) is written in the form :

$$\begin{aligned}
& (\alpha - \kappa_0 - i\delta) \frac{H_1(j,k) + H_1(j+1,k)}{2} \\
& = \frac{H_1(j+1,k) - H_1(j,k)}{d} - i \frac{\kappa_1}{2} \frac{H_2(j,k) + H_2(j,k+1)}{2} \\
& - i \frac{\kappa_1}{2} \frac{H_6(j,k) + H_6(j,k+1)}{2} + i \frac{\kappa_2}{2} \frac{H_3(j,k) + H_3(j-1,k+1)}{2} \\
& + i \frac{\kappa_2}{2} \frac{H_5(j,k) + H_5(j,k+1)}{2} + (i\kappa_3 - \kappa_0) \frac{H_4(j,k) + H_4(j+1,k)}{2}
\end{aligned} \tag{2.37}$$

where d is the side length of one segment, and j and k denote the index along the x direction and the direction of $+60^\circ$ with respect to the x axis, respectively.

At all the surrounding boundaries, we set the facet reflection to zero :

$$\begin{aligned}
& H_1(-\frac{L}{2}, y) = H_1(-\frac{L}{2} + n, -n) = H_4(\frac{L}{2}, y) = H_4(\frac{L}{2} - n, +n) \\
& = H_2(x, -\frac{L}{2}) = H_2(-n, -\frac{L}{2} + n) = H_5(x, \frac{L}{2}) = H_5(n, \frac{L}{2} - n) \\
& = H_3(x, -\frac{L}{2}) = H_3(\frac{L}{2}, y) = H_6(x, \frac{L}{2}) = H_6(-\frac{L}{2}, y) = 0
\end{aligned} \tag{2.38}$$

where L is the length of a triangular photonic crystal cavity and n is the positive integer. By solving the eigenvalue problem for the sets of difference equations, we obtain the eigenvalue $(\alpha - \kappa_0 - i\delta)$ and the eigenvectors $(H_1(j,k), H_2(j,k),$

$H_3(j,k), H_4(j,k), H_5(j,k), H_6(j,k), etc)$.

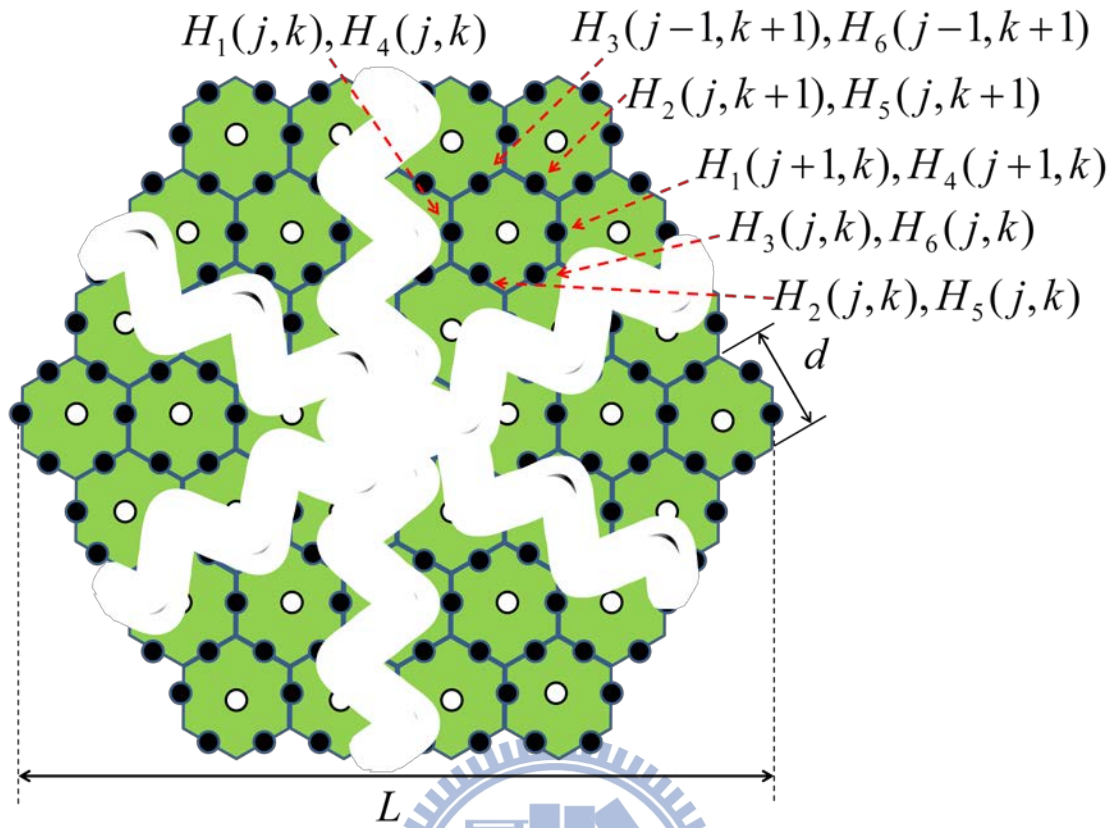
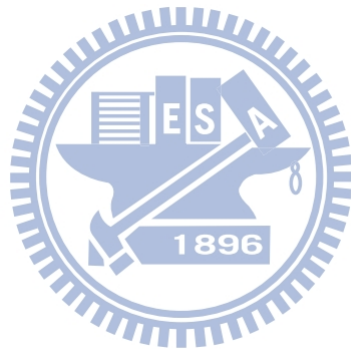


Fig. 2.7 Schematic diagram for triangular lattice for the finite difference method. The target of calculations is carried out at the positions of the white dots by using the complex amplitudes of the neighboring black dots.

References

- [1] K. Sakai, E. Miyai, and S. Noda, *Appl. Phys. Lett.* **89**, 021101 (2006)
- [2] K. Sakai, E. Miyai, and S. Noda, *Opt. Express* **15**, 3981 (2007)
- [3] K. Sakai, J. Yue, and S. Noda, *Opt. Express* **16**, 6033 (2008)
- [4] M. Plihal and A. A. Maradudin, *Phys. Rev. B* **44**, 8565 (1991)
- [5] H. Kogelnik, *Bell Syst. Tech. J.* **48**, 2909 (1969)
- [6] I. Vurgaftman and J. R. Meyer, *IEEE J. Quantum Electron.* **39**, 6, 689 (2003)
- [7] R. F. Kazarinov and C. H. Henry, *IEEE J. Quantum Electron.* **21**, 2, 144 (1985)



Chapter 3

Simulation Results of Photonic Crystal Surface Emitting Lasers

Numerical results

In this chapter, we would discuss the numerical results by solving the complex simultaneous equations based on the coupled wave theory for square lattice and triangular lattice, respectively. The normalized frequency deviation from the Bragg condition, threshold gain and near field patterns of the resonant modes in the 2D PC structure for both square and triangular lattice have been calculated. In addition, the relation between the mode pattern and different coupling strengths are also calculated. Besides, we have evaluated the threshold gain, the normalized frequency deviation and the coupling constants as a function of the hole-filling factor for the fundamental modes. Finally, we would discuss the influence of the coupling constant κ_0 to different band-edge modes.

3.1.1 Mode spectra and mode patterns for square lattice

The typical band structure of photonic crystal for square lattice with transverse electric (TE) polarization shows as Fig. 3.1. And Fig. 3.2 shows the detailed band structure around the Γ point where surface emission is obtained. At the band edges of the band structure is easier to form the resonant mode oscillation. The lasing oscillation at the mode will occur with the lowest threshold and the smallest optical loss [1]. By the reason, calculation of the threshold gain for different resonant modes at the band edges point is very important for understanding of the PCSEL characteristics.

We know that the lasing action is easier to achieve the threshold gain at the Γ point of the band structure. There are three fundamental modes that is A mode, B mode and E mode of doubly degenerate as shown in Fig 3.2. We employing the following parameters in the PC model : the holes dielectric constants $\epsilon_a = 9.8$, the background dielectric constants $\epsilon_b = 12.0$, the gain perturbation $(\alpha_a - \alpha_b) = 0$, the hole filling factor $f = 0.18$, the lattice period $a = 290nm$, and the PC cavity length $L = 50\mu m$. The hole filling factor f define that a circular hole area in the unit cell occupied area ratio. According to the numerical solution of the calculation, we plot the threshold gain as a function of frequency deviation from the Bragg condition for the resonant modes, as shown in Fig. 3.3(a). We classify the groups of resonances as $N = \pm 1, \pm 2, \pm 3, \dots$ according to their frequency deviation from the Bragg condition, where N is the mode number [2]. The more detailed plots for modes $N = -1$ and $N = 1$ are shown in Fig. 3.3(b) and Fig. 3.3(c), respectively.

The eigenvectors of Eq. (2.20) provide the complex amplitudes such as R_x , S_x , R_y , and S_y , which are functions of the positions x and y . The intensity envelope

(mode pattern) of the resonant mode throughout the PC structure can be determined from these amplitudes using the sum $R_x R_x^* + S_x S_x^* + R_y R_y^* + S_y S_y^*$.

It could be classified that the mode A ($\alpha L = 0.46597, \delta L = -6.1259$), mode B ($\alpha L = 0.57709, \delta L = -4.8881$), and mode E ($\alpha L = 1.7107, \delta L = 4.4137$) are fundamental modes that have a single-lobed intensity pattern throughout the photonic crystal, as shown in Fig. 3.4(a-d). We could understand that the lowest frequency of these three modes is mode A and mode E is doubly degenerate. Modes A and B have twin modes A_0 ($\alpha L = 1.6768, \delta L = 4.3506$) and B_0 ($\alpha L = 1.751, \delta L = 4.4847$), respectively. Modes A_0 and B_0 exhibit vase-like patterns with zero intensity at the center of the structure, as shown in Fig. 3.4(e-f). The other points in Fig. 3.3(b) and Fig. 3.3(c) correspond to higher order modes which consist of a higher order transverse mode. A lot of higher order modes in the proximity of mode E are almost impossible to distinguish in Fig. 3.3(c). Then, the numerical results of the threshold gain for modes A, B, and E by calculation are $\alpha_A L = 0.46597$, $\alpha_B L = 0.57709$, and $\alpha_E L = 1.7107$, respectively. As a result, mode A has the lowest threshold gain and could easily achieve the lasing oscillation.

Fig. 3.4(g) (*ex.* $\alpha L = 0.5522, \delta L = -5.4595$ or $\alpha L = 1.7094, \delta L = 4.4125 \dots$) and Fig. 3.4(h) (*ex.* $\alpha L = 0.53445, \delta L = -5.4781$ or $\alpha L = 1.7103, \delta L = 4.4133 \dots$) illustrates the intensity envelope for the higher order modes around mode E, which have several nodes and antinodes. Fig. 3.4(i) (*ex.* $\alpha L = 0.5175, \delta L = -5.5065$ or $\alpha L = 0.59833, \delta L = -5.3942 \dots$) and Fig. 3.4(j) (*ex.* $\alpha L = 1.3382, \delta L = -7.7656$ or $\alpha L = 1.2426, \delta L = -8.3053 \dots$) show like the two-lobe pattern and four-lobe pattern, respectively, which are the intensity envelope for the higher order modes. The envelopes of other higher order modes also exhibit a series of nodes and antinodes.

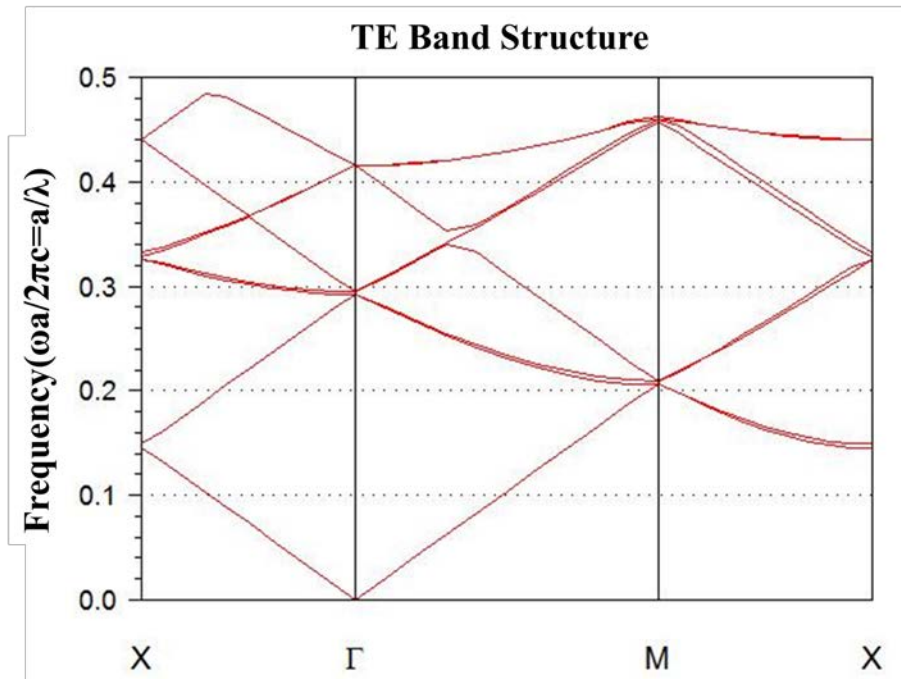


Fig. 3.1 Band structure for square lattice photonic crystal with TE polarization

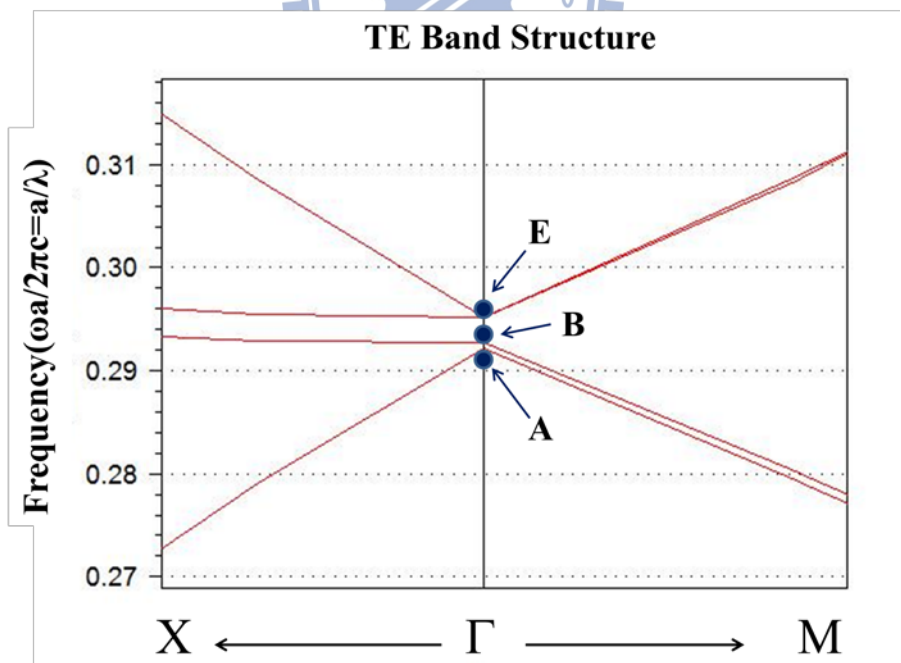


Fig. 3.2 The detailed band structure in the proximity of the Γ - point for square lattice

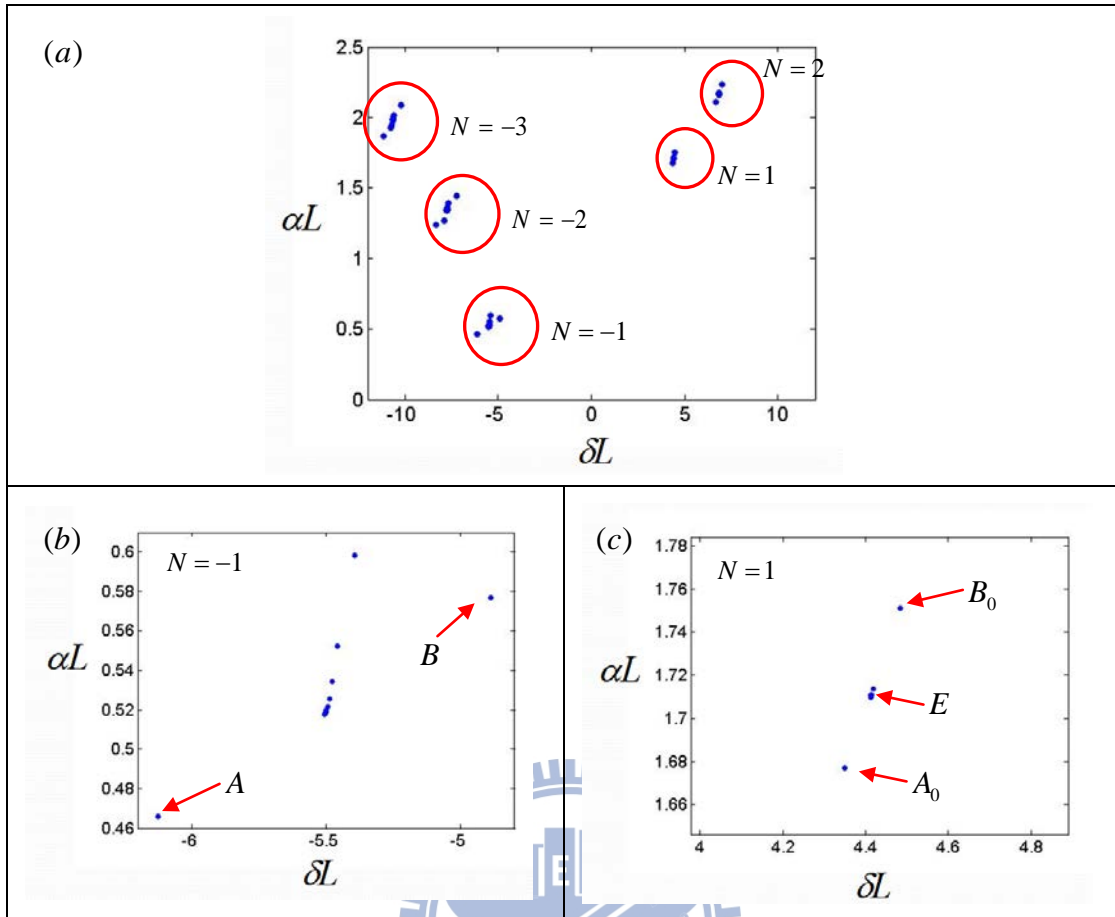
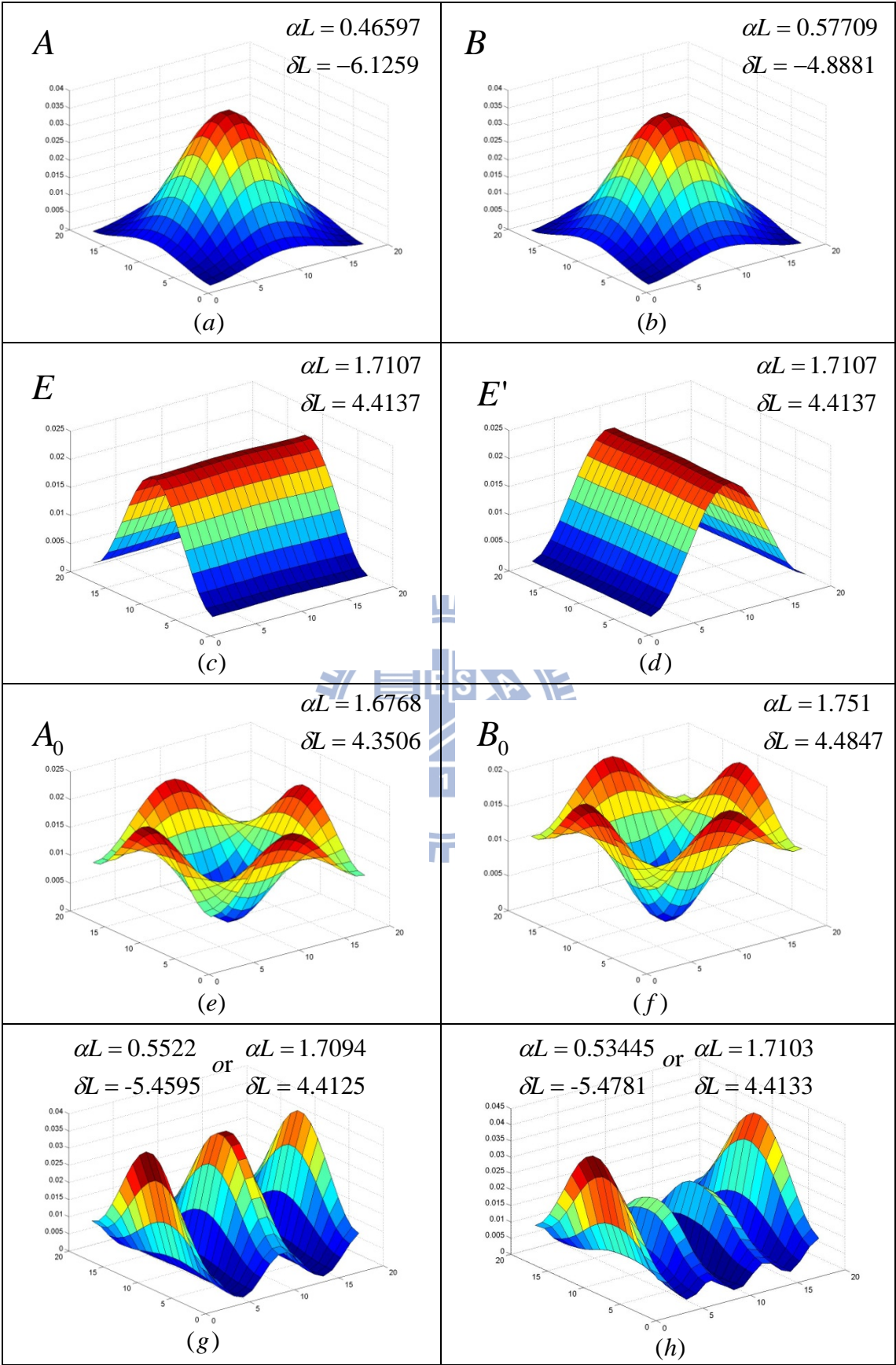


Fig 3.3 (a) Threshold gain as a function of frequency deviation from the Bragg condition for square lattice (b) Magnified plot for modes $N = -1$, and (c) for $N = 1$



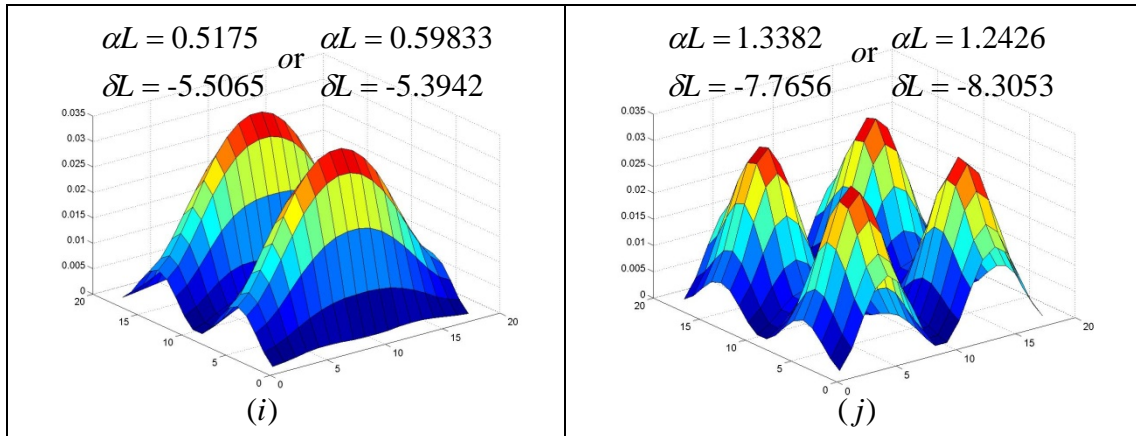


Fig 3.4 (a-d) Mode pattern for square lattice for the fundamental modes (A, B, and E), respectively, (e-f) spatial intensity distributions A_0 and B_0 , and (g-j) mode pattern for the higher order modes



3.1.2 Threshold gain as a function of hole filling factor for square lattice

The coupling constants are a function of filling factor f and hence the threshold gain should also be strongly dependent on filling factor f . Fig. 3.5 shows the coupling constants as a function of the hole filling factor. We note that κ_3 becomes zero at $f = 0.3$, which implies that the backward diffraction vanishes. Fig. 3.7 shows the threshold gain of the fundamental modes A, B, and E as a function of hole filling factor. The threshold gain for modes A and B drastically increases in the region of $f = 0.3$. This is because the degree of backward diffraction becomes very weak and is insufficient for optical oscillation. This result indicates that the coupling constant κ_3 is the dominant factor determining the degree of optical confinement in the current system, a square lattice with TE polarization.

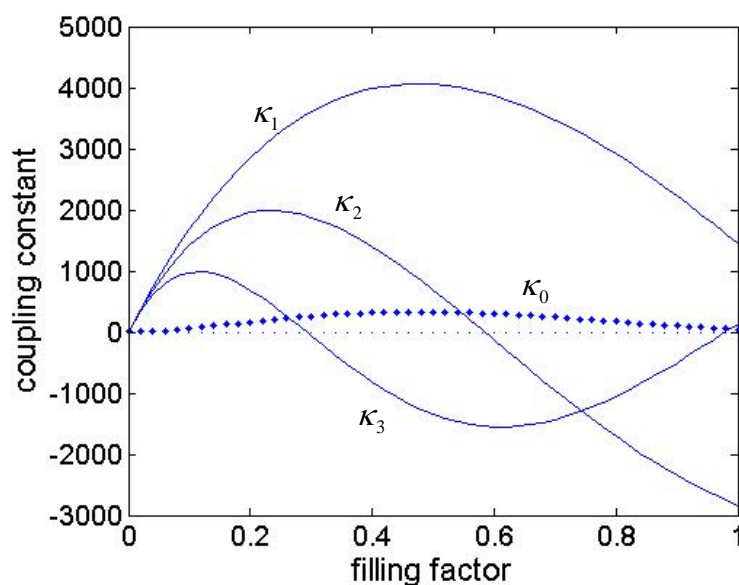


Fig 3.5 Coupling constants as a function of hole filling factor for square lattice

To elucidate the origin of the threshold difference among the fundamental modes, we calculated the threshold gain for zero surface emission ($\kappa_0 = 0$) as shown in Fig. 3.8 and Fig. 3.9. It is quite obvious that the average of the threshold gain to consider the surface emission κ_0 is higher than the average of the threshold gain not to consider the surface emission κ_0 for the fundamental modes A, B, and E, as compared with Fig. 3.7 and Fig. 3.9. In this case, the threshold gain of mode E greatly decreased and the threshold gain between mode E and mode A(or B) is similar, as shown in Fig. 3.9. Thus, the major of loss for mode E is surface emission. The difference in threshold gain between modes A and B in Fig. 3.7 indicates that the emission loss from the edges of the cavity differs. The frequency deviation from the Bragg condition don't have much influence of the surface emission κ_0 , as compared with Fig. 3.6 and Fig. 3.8.

In Fig. 3.7, the lowest threshold gains of square PCSELS for A, B and E mode are observed at filling factor =0.6,0.6 and 0.05, respectively. The 2D coupling induces the curves splitting for modes A and B. Therefore, we could observe a highly mode selection with stronger 2D coupling. Besides, in Fig. 3.6, the curves splitting in frequency between mode A (or B) and mode E is induced by backward vector of coupling constant κ_3 . This splitting corresponds to the stopband in 1D DFB lasers, which is induced by coupling between the counter propagating waves.

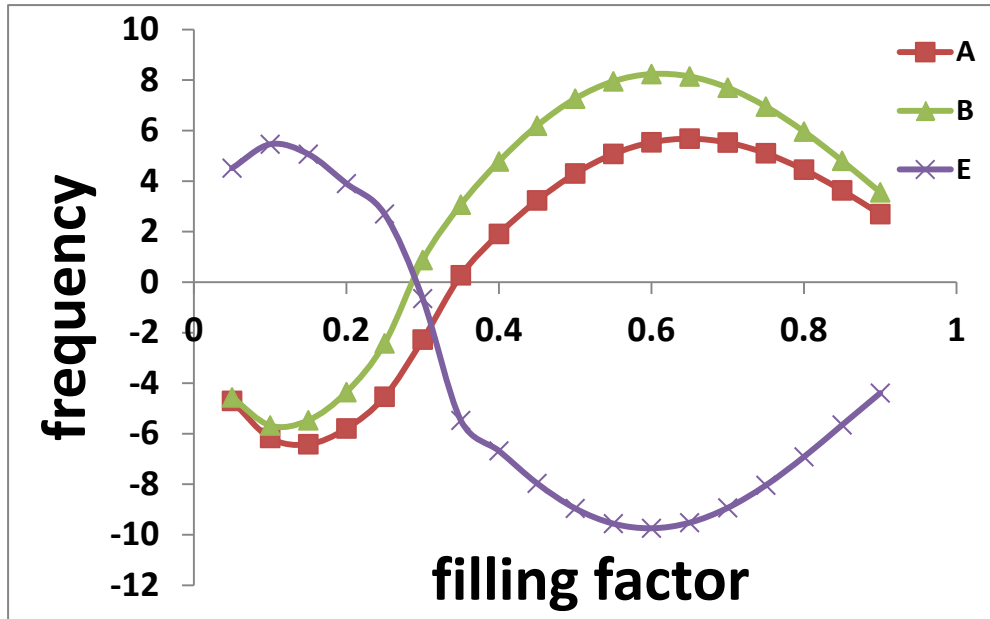


Fig 3.6 The frequency deviation as a function of hole filling factor of the fundamental modes A, B and E for square lattice for considering surface emission $\kappa_0 \neq 0$

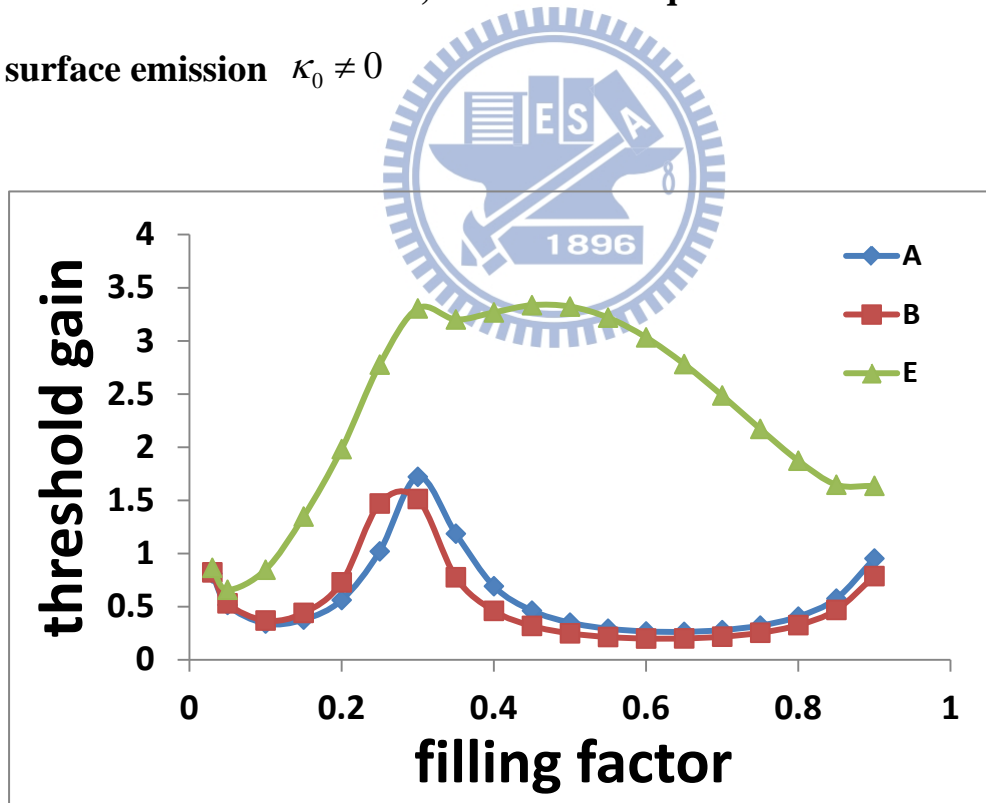


Fig 3.7 The threshold gain as a function of hole filling factor of the fundamental modes A, B and E for square lattice for considering surface emission $\kappa_0 \neq 0$

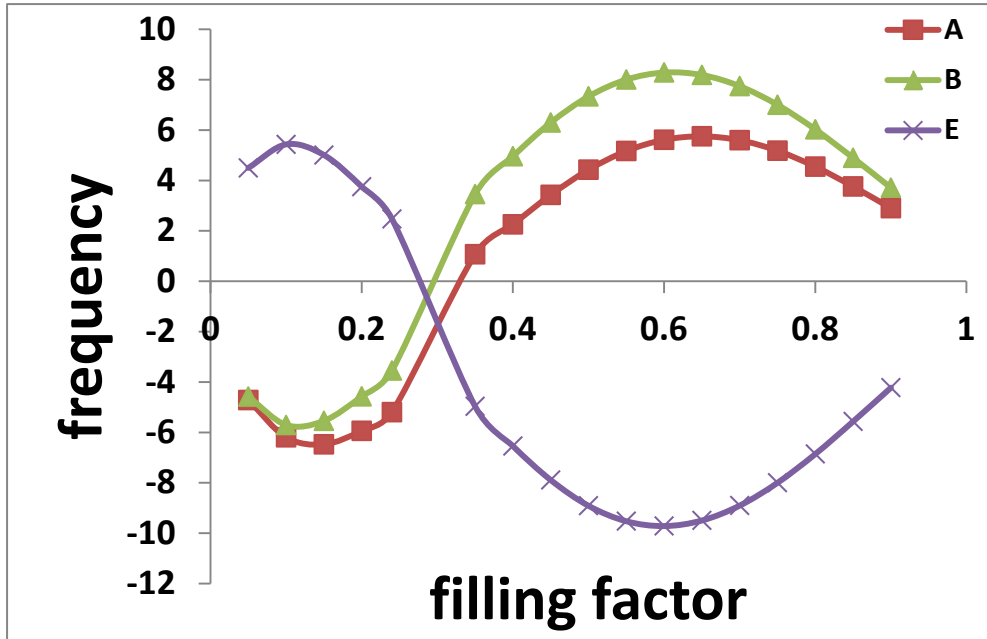


Fig 3.8 The frequency deviation as a function of hole filling factor of the fundamental modes A, B and E for square lattice for zero surface emission $\kappa_0 = 0$

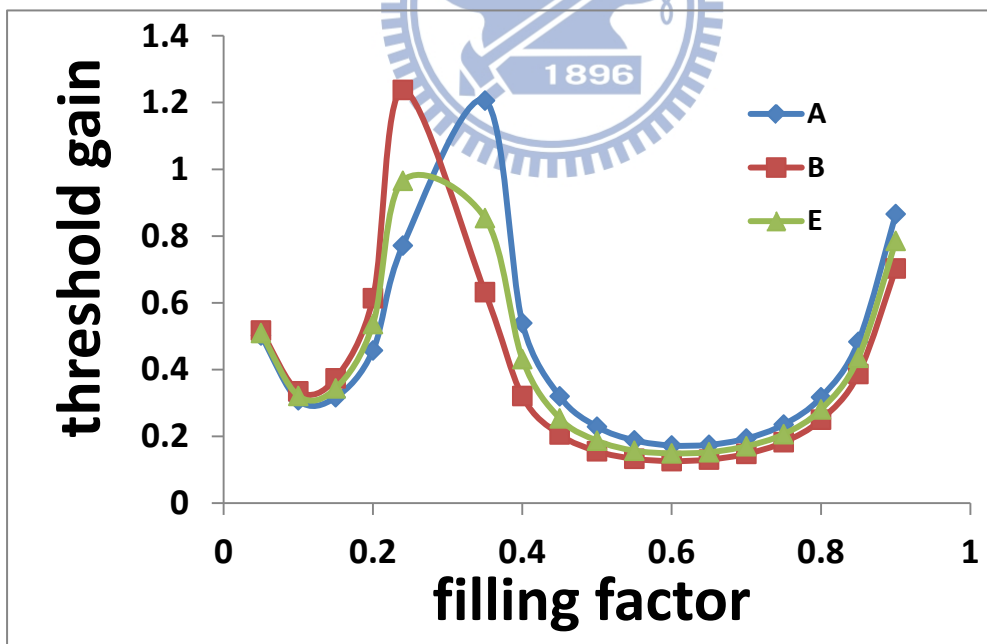


Fig 3.9 The threshold gain as a function of hole filling factor of the fundamental modes A, B and E for square lattice for zero surface emission $\kappa_0 = 0$

3.2.1 Mode spectra and mode patterns for triangular lattice

The typical band structure of photonic crystal for triangular lattice with transverse electric (TE) polarization shows as Fig. 3.10. Fig. 3.11 shows the detailed band structure around the Γ point where surface emission is obtained. At the band edges of the band structure is easier to form the resonant mode oscillation.

We know that the lasing action is easier to achieve the threshold gain at the Γ point of the band structure. There are four fundamental modes including A mode, B mode, C mode and D mode, as shown in Fig 3.11. B mode and D mode are the mode of doubly degenerate, respectively. We import the following parameters in the PC model : the holes dielectric constants $\varepsilon_a = 9.8$, the background dielectric constants $\varepsilon_b = 12.0$, the gain perturbation $(\alpha_a - \alpha_b) = 0$, the hole filling factor $f = 0.37$, the lattice period $a = 290nm$, and the PC cavity length $L = 50\mu m$. The hole filling factor f define that a circular hole area in the unit cell occupied area ratio. According to the numerical solution of the calculation, we plot the threshold gain as a function of frequency deviation from the Bragg condition for the resonant modes are shown in Fig. 3.12.

The eigenvectors of Eq. (2.36) provide the complex amplitudes such as H_1 , H_2 , H_3 , H_4 , H_5 , and H_6 , which are functions of the positions x and y . The intensity envelope (mode pattern) of the resonant mode throughout the PC structure can be determined from these amplitudes using the sum $H_1H_1^* + H_2H_2^* + H_3H_3^* + H_4H_4^* + H_5H_5^* + H_6H_6^*$.

It could be classified that mode A ($\alpha L = 2.0388, \delta L = -11.118$), mode B ($\alpha L = 0.87575, \delta L = -2.7631$), mode C ($\alpha L = 0.77078, \delta L = 12.3982$) and mode D ($\alpha L = 1.9519, \delta L = 2.1771$) are fundamental modes, each mode have a single-lobed

intensity pattern throughout the photonic crystal, as shown in Fig. 3.13(a-f). We can identify that the lowest frequency of these four modes is mode A, as shown in Fig. 3.11. At the same time, we can find the six mode patterns for fundamental modes which show similarly single-lobed intensity patterns. This observation of the six mode patterns can be found by doubly degenerate into two categories. The frequency of the band structure, as shown in Fig. 3.11, can be helped to distinguish the different modes. The numerical results of the threshold gain for modes A, B, C, and D are $\alpha_A L = 2.0388$, $\alpha_B L = 0.87575$, $\alpha_C L = 0.77078$ and $\alpha_D L = 1.9519$, respectively. As a result, mode C has the lowest threshold gain and could easily achieve the lasing oscillation.

Fig. 3.13(g-j) illustrates the intensity envelope for the higher order modes, which have several nodes and antinodes. Fig. 3.13(g) illustrates that the phase of intensity envelope of the resonant mode is flipped as crossing a given axis. This produces a mode pattern that only exist two lobes. On the other hand, Fig. 3.13(h) illustrates that the phase of intensity envelope of the resonant mode is flipped as crossing two given axes. This produces a mode pattern that exist four lobes. In the Fig. 3.13(i), it shows that the intensity envelope characteristic with six peaks spaced almost evenly around the perimeter of the annulus. For this mode, the phases of the six field components alternate as a function of azimuthal angle that there are not two of adjacent components separated by 60° constructive interference [3]. Finally, Fig. 3.13(j) illustrates that the intensity envelope characteristic forms an annular pattern. The modes shown in Fig. 3.13(g-i) may be classified as out-of-phase, since pronounced destructive interference in the surface-emitted component substantially reduces the output power and also degrades the beam quality. The envelopes of other higher order modes also exhibit a series of nodes and antinodes.

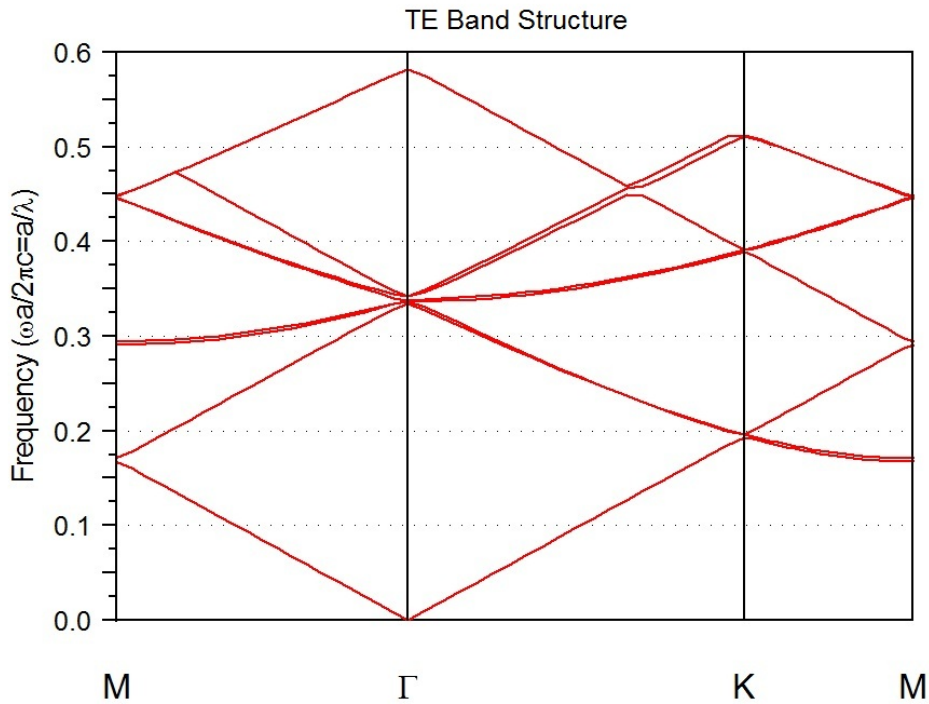


Fig. 3.10 Band structure for triangular lattice photonic crystal with TE polarization

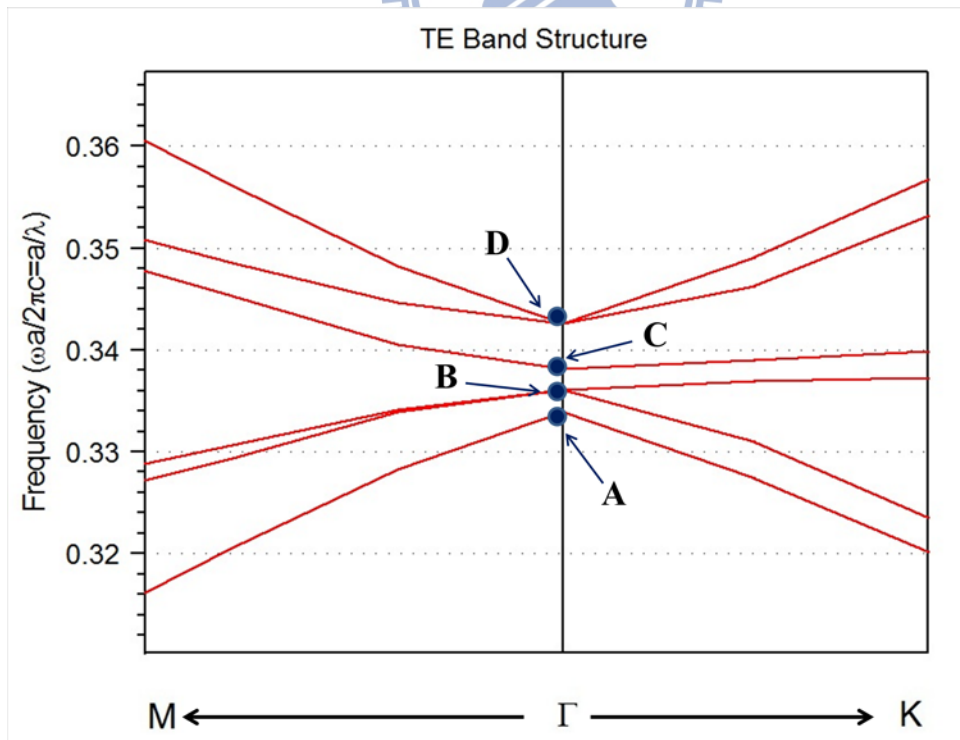


Fig. 3.11 The detailed band structure in the proximity of the Γ -point for triangular lattice

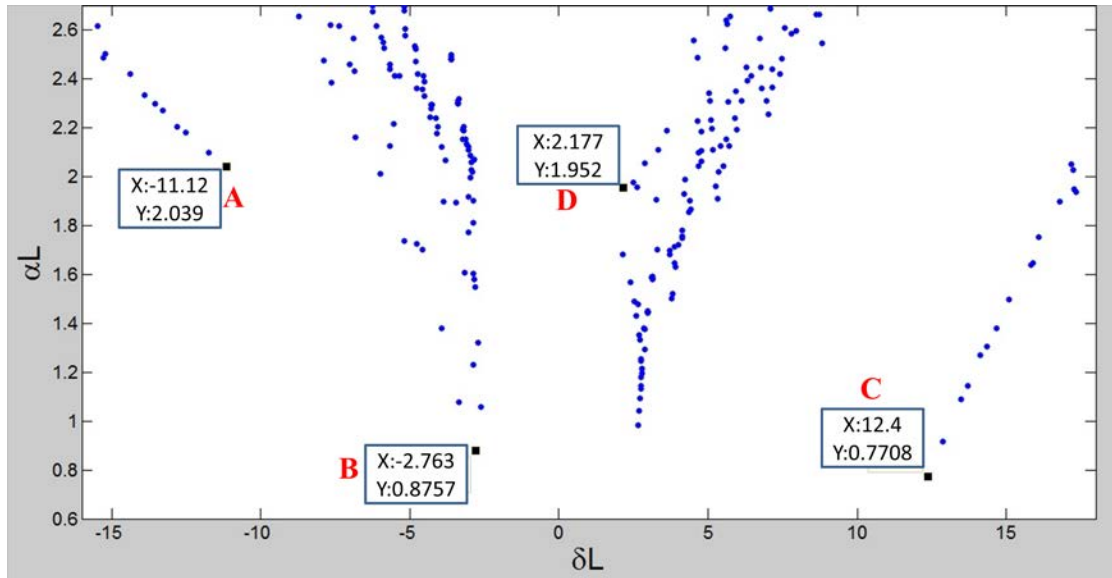
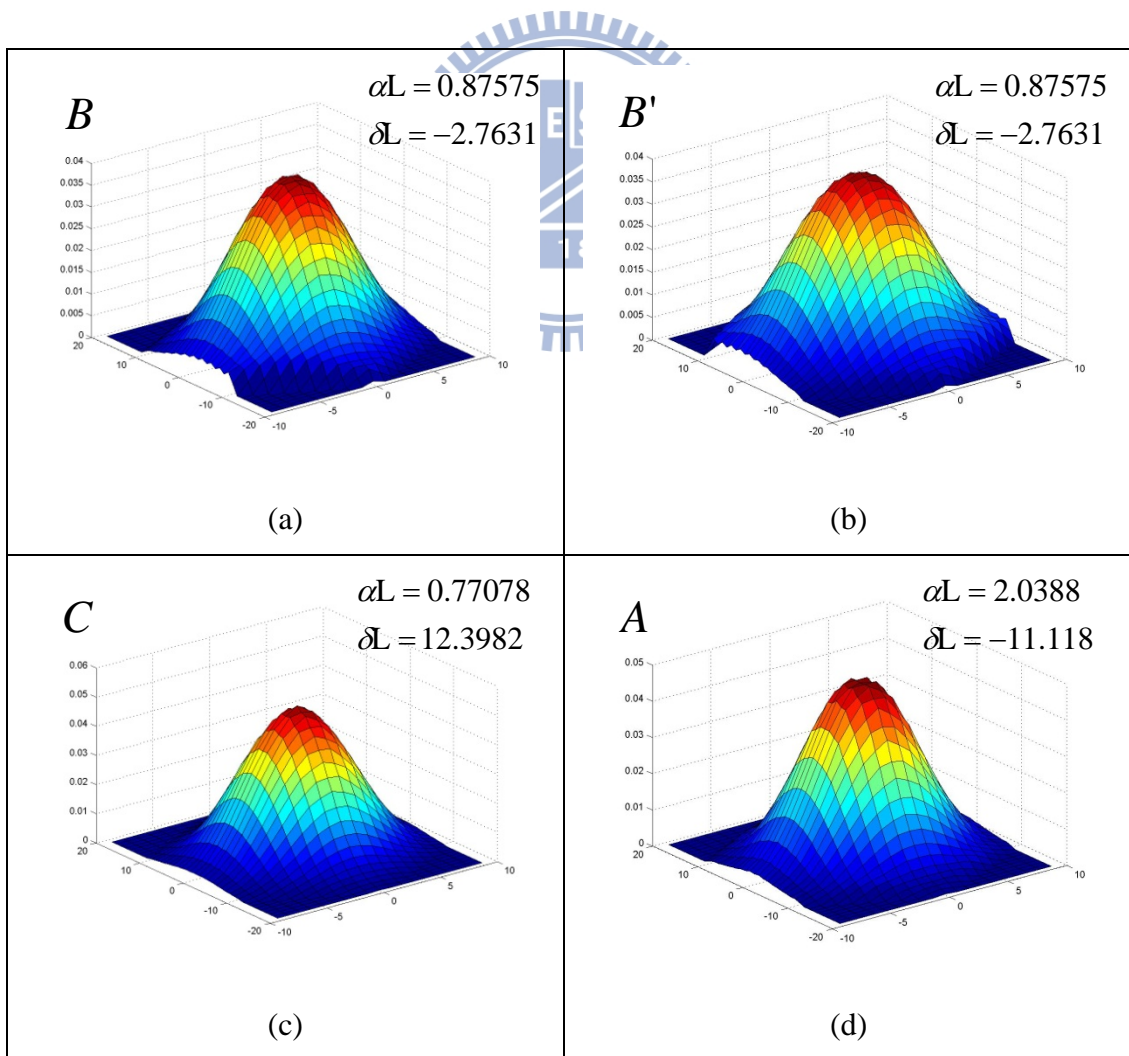


Fig 3.12 Threshold gain as a function of frequency deviation from the Bragg condition for triangular lattice



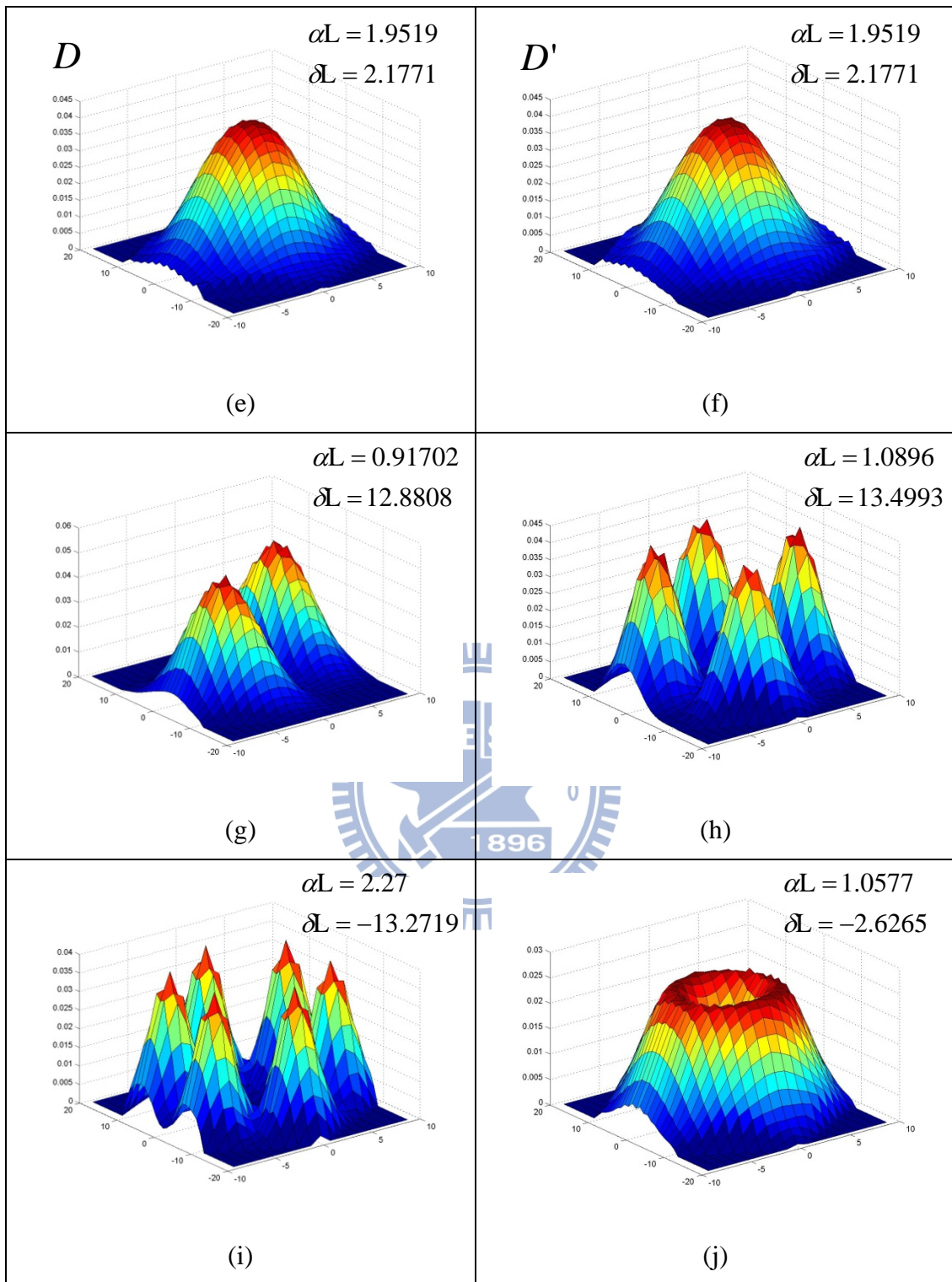


Fig 3.13 (a-f) Mode pattern for triangular lattice for the fundamental modes (A, B, C, and D), respectively and (g-j) mode pattern for the higher order modes

3.2.2 Threshold gain as a function of hole filling factor for triangular lattice

The coupling constants are calculated as a function of filling factor f and hence the threshold gain should also be strongly dependent on filling factor f . Fig. 3.14 shows the coupling constants as a function of the hole filling factor. It should be noted that κ_3 becomes zero at $f = 0.25$, which implies that the backward diffraction vector is vanished. The threshold gain could be affected by this factor. On the other hand, the κ_0 has the maximum value at $f = 0.45$ which implies that this condition has the maximum radiation loss. We could also obtain that κ_2 and κ_3 have the maximum value at $f = 0.15$, κ_1 and κ_0 have the maximum value at $f = 0.45$, and κ_2 becomes zero at $f = 0.35$.

Fig. 3.18 shows the threshold gain of the fundamental modes A, B, C and D as a function of hole filling factor. It is clearly the threshold gain for modes C and D

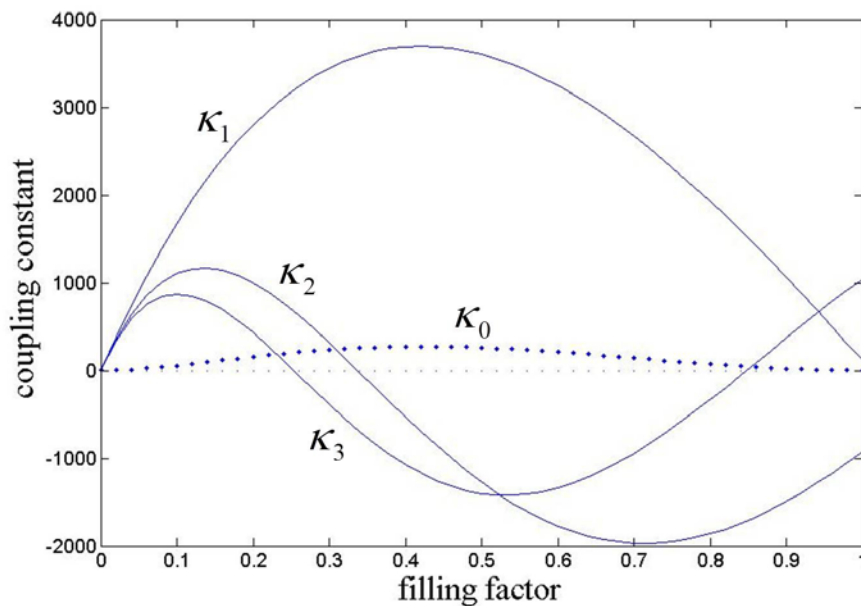


Fig 3.14 Coupling constants as a function of hole filling factor for triangular lattice

drastically increases in the region of $f = 0.25$. It is because the degree of backward diffraction vector becomes very weak and is insufficient for optical oscillation. This result indicates that the coupling constant κ_3 is the mainly factor of determining the degree for optical resonant in the current system.

Fig. 3.15 and Fig. 3.16 show that the frequency deviation and threshold gain as a function of hole filling factor of the fundamental modes A, B, C and D for triangular lattice with considering surface emission κ_0 , respectively. The threshold gain of mode A and B have the lowest value at $f = 0.12$ in Fig 3.16. It is because the coupling constant κ_2 and κ_3 are the maximum value and could provide sufficient optical resonant. At the same time, the threshold gain for mode A and D has the local maximum value at $f = 0.45$, because the coupling constant κ_0 and κ_1 are the maximum value which would increase the optical loss. In particular, the threshold gain of fundamental modes becomes larger when the hole filling factor f approach zero or one. In this case, the photonic crystal is without any function.

To elucidate the originally difference among the fundamental modes, we calculated the threshold gain and frequency deviation as a function of filling factor for zero surface emission ($\kappa_0 = 0$), as shown in Fig. 3.17 and Fig. 3.18. It is obviously that all of the threshold gain with considering surface emission κ_0 is higher than that without surface emission κ_0 for the fundamental modes A, B, C and D. In Fig. 3.18, by compared with these two conditions (with or without κ_0), the curves of the threshold gain for mode A and D at $f = 0.45$ show smooth tendency instead of violent variation in Fig. 3.16 indicating that the threshold gain for mode A and D are mainly affected by the coupling constant κ_0 . The influence of radiation loss κ_0 is

larger than the coupling constant κ_1 for these two modes. At the same time, the curve of threshold gain of mode A is similar with mode B for zero surface emission, as shown in Fig. 3.18. The mainly difference between the threshold gain of mode A and B for surface emission is shown in Fig. 3.16. It can be seen the curve of mode A is gradually increased with considering κ_0 . Thus, the influence of surface emission factor for mode A is larger than mode B. As for the deviation frequency for mode A, B, C and D without considering κ_0 , the tendency of each mode shows similar curves between Fig. 3.15 and Fig. 3.17. It indicates that the frequency deviation from the Bragg condition does not affect by the surface emission factor κ_0 .

At last, we could finalize these results of threshold gain for each mode. In Fig. 3.16, the lowest threshold gains of triangular PCSEs for A, B, C and D mode are observed at filling factor =0.1, 0.1, 0.05 and 0.05, respectively. The surface emission coupling induces the curves splitting for modes A and B. Therefore, we could observe a highly mode selection with stronger 2D coupling. In Fig. 3.15, the curves splitting in frequency between mode A (or B) and mode C(or D) is induced by backward vector of coupling constant κ_3 . This splitting corresponds to the stopband in 1D DFB lasers, which is induced by coupling between the counter propagating waves.

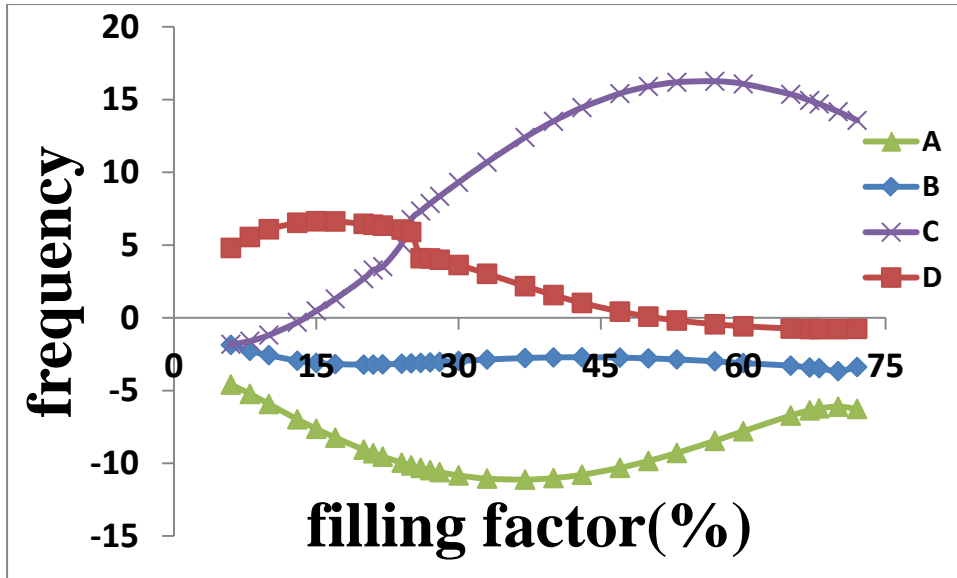


Fig 3.15 The frequency deviation as a function of hole filling factor of the fundamental modes A, B, C and D for triangular lattice for considering surface emission $\kappa_0 \neq 0$

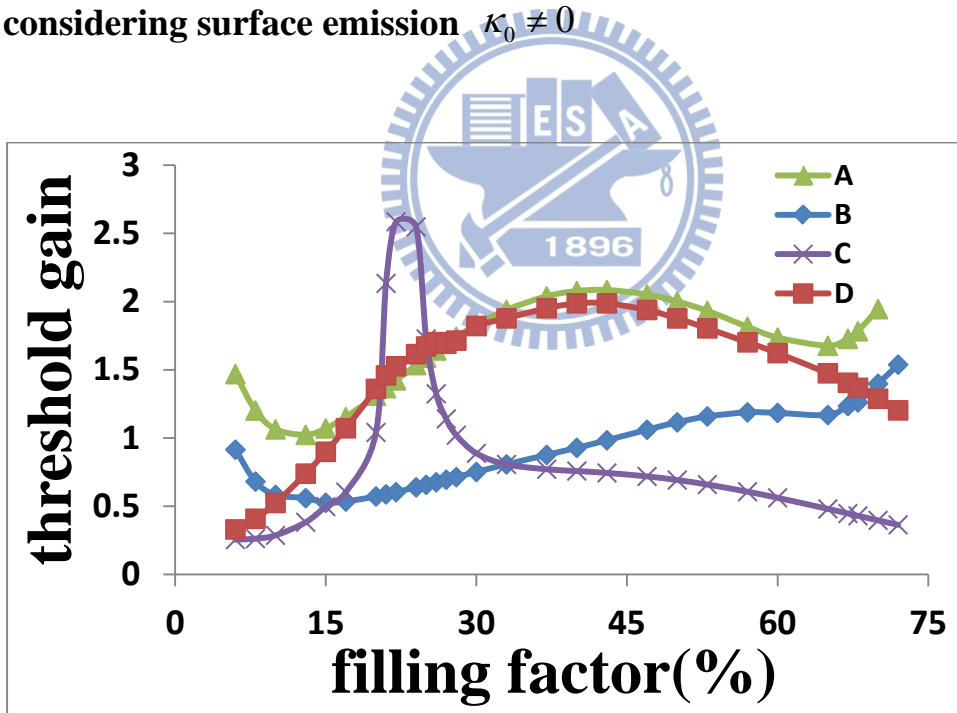


Fig 3.16 The threshold gain as a function of hole filling factor of the fundamental modes A, B, C and D for triangular lattice for considering surface emission $\kappa_0 \neq 0$

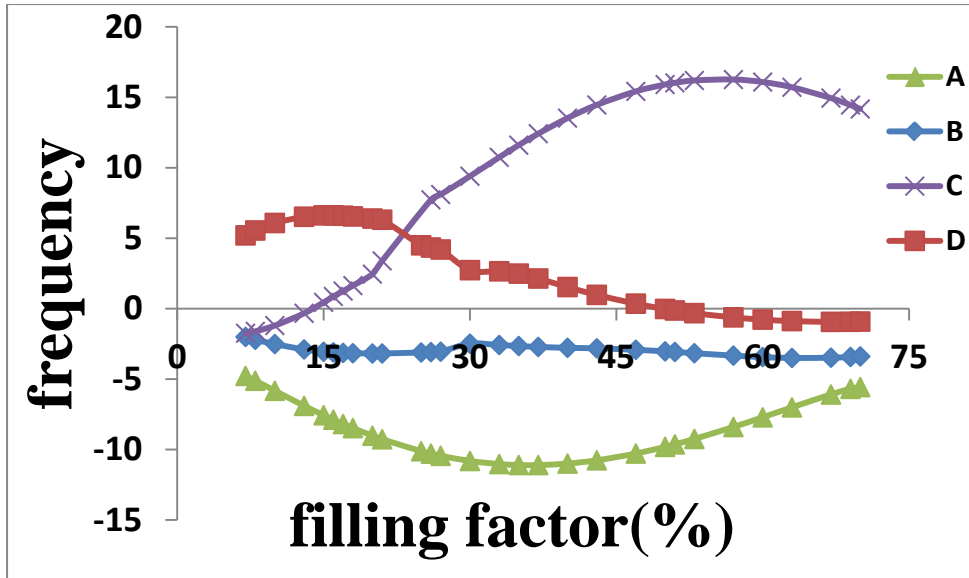


Fig 3.17 The frequency deviation as a function of hole filling factor of the fundamental modes A, B, C and D for triangular lattice for zero surface emission $\kappa_0 = 0$

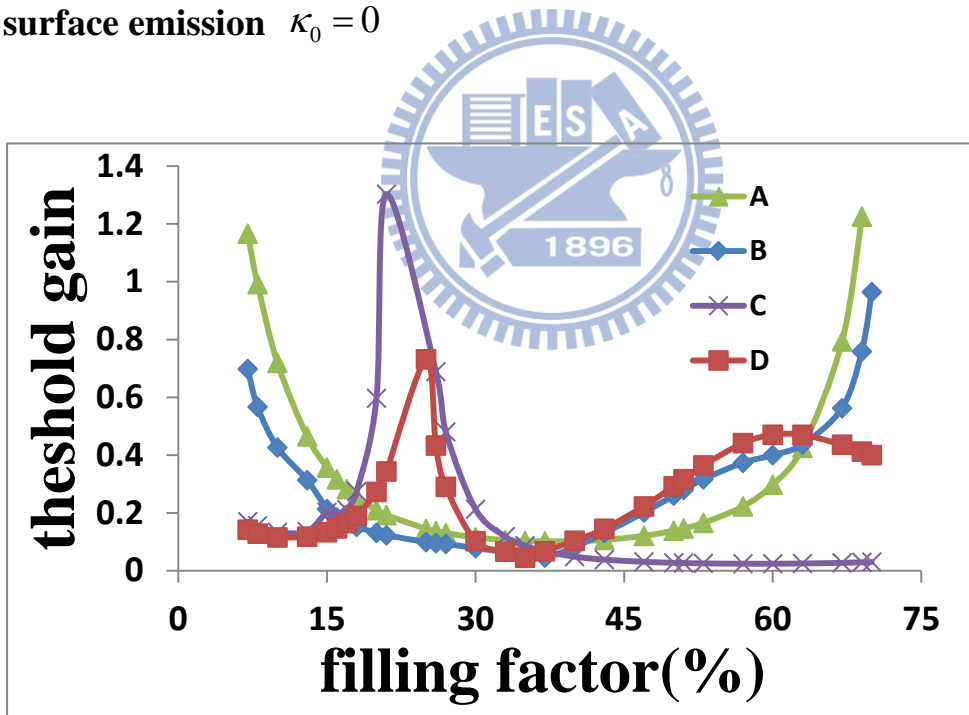
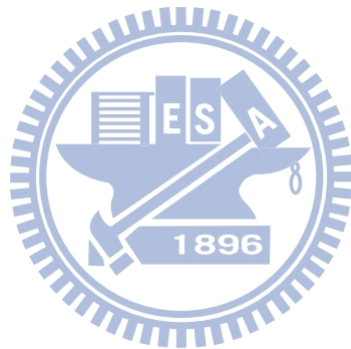


Fig 3.18 The threshold gain as a function of hole filling factor of the fundamental modes A, B, C and D for triangular lattice for zero surface emission $\kappa_0 = 0$

References

- [1] K. Sakai, E. Miyai, T. Sakaguchi, D. Ohnishi, T. Okano, and S. Noda, *IEEE J. Sel. Areas Commun.*, **23**, 7, 1335(2005)
- [2] H. Kogelnik and C. V. Shank, *J. Appl. Phys.*, **43**, 2327 (1972)
- [3] I. Vurgaftman and J. R. Meyer, *IEEE J. Quantum Electron.* **39**, 6, 689 (2003)



Chapter 4

Conclusion

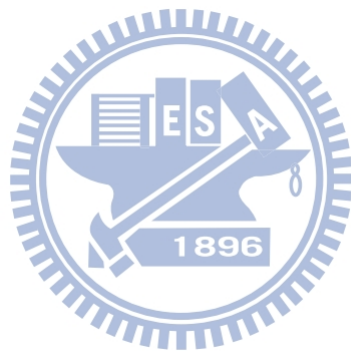
We have developed the coupled wave theory for square lattice and triangular lattice of photonic crystal lasers with transverse electric polarization. Numerical calculations by solving the eigenvalue problem have shown the threshold gain, the frequency deviation and the mode pattern of the 2D resonant modes. The intensity pattern of the fundamental modes was found to depend on the coupling strength, with peaks in intensity at the ends of the structure for weak coupling and maximum intensity at the center for strong coupling.

For square lattice, the lowest threshold gains of PCSELs for fundamental mode A, B and E are observed at filling factor $f=0.6$, 0.6 and 0.05 , respectively. The surface emission κ_0 and backward coupling κ_3 are the dominant factor of determining the degree of optical confinement in the current system for the fundamental mode. The surface emission coupling constant κ_0 induces the curve splitting between modes A (or B) and E.

As for triangular lattice, the lowest threshold gains of PCSELs for fundamental mode A, B, C and D are observed at filling factor $f=0.1$, 0.1 , 0.05 and 0.05 , respectively. The surface emission κ_0 and backward coupling κ_3 are the dominant factor of determining the degree of optical confinement in the current system for the fundamental mode. The surface emission coupling constant κ_0 induces the curve splitting between modes A and B. Therefore, we could observe a highly mode selection with stronger 2D coupling.

The out of plane radiation of photonic crystal has been considered by coupling

coefficient κ_0 , and it has massive influence to threshold gain of PCSELS. The results obtained in this thesis provide fundamental insight into the 2D DFB effect of the PC lasers. To fabricate low threshold gain PCSELS, coupled wave theory provides us a more convenient and faster method to modify our designs. A further development in designing and optimizing the 2D PC lasers by the current method is envisaged.



Appendix Code (in Matlab System)\

Mode patterns of photonic crystal with square lattice

```

clc
clear
L=50*10^(-4);           % length of PC cavity
Epsa=9.8;               % dielectric constants of the circular holes
Epsb=12.0;              % dielectric constants of the background
a=290*10^(-7);         % lattice constant
b=2*pi/a;               % wave number
%-----coupling constant-----
G=[b sqrt(2)*b 2*b];
z2=1;
for z1=1:3
    f(z2)=0.18;         % filling factor
    r(z2)=a*sqrt(f(z2)/(pi));
    Eps0(z2)=sqrt(Epsa*f(z2)+Epsb*(1-f(z2)));
    kG(z2)=0.2841*(-(pi)*(Epsa-Epsb)/(a*Eps0(z2)))^2*f(z2)*
    BESSEL(1,G(z1)*r(z2))/(G(z1)*r(z2));
    kG(isnan(kG))=1;
    if z1==1
        kG1(z2)=kG(z2);
        k0(z2)=2*kG1(z2)*kG1(z2)*L/500;
    end
    k(z1)=kG(z2);
end
%-----kappa variable-----
n=18;                   % even
k1=k(1);
k2=k(2);
k3=k(3);
%-----parameter-----
A=(i*4*(k1)^2)/b;
C=i*2*(k1^2)/b;
B=i*(k3)-k0;
d=L/n;
%-----boundary & phase shift-----
ro=0.0;
phi=0*pi;
phs=pi*0/18;
brro=ro;
brph=phi;
blo=ro;
blph=phi;
buro=0;
buph=phi;
bdro=0;
bdph=phi;
%-----matrix-----
A11=(0.5*A+1/d)*eye(n)+diag((0.5*A-1/d)*ones(1,n-1),-1);
A11(n,n)=A11(n,n)+0.5*B*brro*exp(i*brph);
Mn11=kron(eye(n),A11);
A12=(0.5*B)*eye(n)+diag((0.5*B)*ones(1,n-1),1);
A12(1,1)=A12(1,1)+(0.5*A-1/d)*blo*exp(i*blph);
P=diag([exp(-i*phs)*ones(1,n/2) exp(i*phs)*ones(1,n/2)]);
M12=kron(eye(n),P*A12);
A13=diag(0.5*C*buro*exp(i*buph)*[zeros(1,n*(n-1))
ones(1,n)]);
M13=(0.5*C)*eye(n*n)+diag((0.5*C)*ones(1,n*n-n),-n)+A13;
A14=diag(0.5*C*bdro*exp(i*bdph)*[ones(1,n)
zeros(1,n*(n-1))]);
M14=(0.5*C)*eye(n*n)+diag((0.5*C)*ones(1,n*n-n),n)+A14;
A21=(0.5*B)*eye(n)+diag((0.5*B)*ones(1,n-1),-1);
A21(n,n)=A21(n,n)+(0.5*A-1/d)*brro*exp(i*brph);
Q=diag([exp(i*phs)*ones(1,n/2) exp(-i*phs)*ones(1,n/2)]);
M21=kron(eye(n),Q*A21);
A22=(0.5*A+1/d)*eye(n)+diag((0.5*A-1/d)*ones(1,n-1),1);
A22(1,1)=A22(1,1)+(0.5*B)*blo*exp(i*blph);
Mn22=kron(eye(n),A22);
%-----

```

```

A31=(0.5*C)*eye(n)+diag((0.5*C)*ones(1,n-1),-1);
A31(n,n)=A31(n,n)+(0.5*C)*brro*exp(i*brph);
M31=kron(eye(n),Q*A31);
A32=(0.5*C)*eye(n)+diag((0.5*C)*ones(1,n-1),1);
A32(1,1)=A32(1,1)+(0.5*C)*blro*exp(i*blph);
M32=kron(eye(n),P*A32);
A33=diag((0.5*B)*buro*exp(i*buph)*[zeros(1,n*(n-1))
ones(1,n)]);
Mn33=(0.5*A+1/d)*eye(n*n)+diag((0.5*A-1/d)*ones(1,n*n-
n),-n)+A33;
A34=diag((0.5*A-1/d)*bdro*exp(i*bdph)*[ones(1,n)
zeros(1,n*(n-1))]);
M34=(0.5*B)*eye(n*n)+diag((0.5*B)*ones(1,n*n-n),n)+A3
4;
%-----
A43=diag((0.5*A-1/d)*buro*exp(i*buph)*[zeros(1,n*(n-1))
ones(1,n)]);
M43=(0.5*B)*eye(n*n)+diag((0.5*B)*ones(1,n*n-n),-n)+A4
3;
A44=diag((0.5*B)*bdro*exp(i*bdph)*[ones(1,n)
zeros(1,n*(n-1))]);
Mn44=(0.5*A+1/d)*eye(n*n)+diag((0.5*A-1/d)*ones(1,n*n-
n),n)+A44;
TT=[Mn11 M12 M13 M14;M21 Mn22 M13 M14;M31 M32
Mn33 M34;M31 M32 M43 Mn44];
%-----
R11=eye(n)+diag(ones(1,n-1),-1);
Rn11=kron(eye(n),R11);
R22=eye(n)+diag(ones(1,n-1),1);
Rn22=kron(eye(n),R22);
Rn33=eye(n*n)+diag(ones(1,n*n-n),-n);
Rn44=eye(n*n)+diag(ones(1,n*n-n),n);
Z=zeros(n*n);
R=[Rn11 Z Z Z;Z Rn22 Z Z;Z Z Rn33 Z;Z Z Z Rn44];
Y=inv(R);
T=Y*TT;
[VR D]=eig(T);
realpart=L*(real(2*diag(D)))+k0*L;
imagpart=L*(-imag(2*diag(D)));
figure()
plot(imagpart,realpart,')
axis([-20,20,0,5])
N=find(realpart<1.5);
S=size(N);
%-----Mode pattern Hz-----
for z=1:S(1)
V=VR(:,N(z));
for y=1:n
for x=1:n
if x==1 & y==1
Rx=0;
Sx1=V(n*n+(y-1)*n+x+1);
Ry=0;
Sy1=V(3*n*n+(y)*n+x);
elseif x==1 & y==n
Rx=0;
Sx1=V(n*n+(y-1)*n+x+1);
Ry=V(2*n*n+(y-2)*n+x);
Sy1=0;
elseif x==n & y==1
Rx=V(n*(y-1)+x-1);
Sx1=0;
Ry=0;
Sy1=V(3*n*n+(y)*n+x);
elseif x==n & y==n
Rx=V(n*(y-1)+x-1);
Sx1=0;
Ry=V(2*n*n+(y-2)*n+x);
Sy1=0;
elseif x==1
Rx=0;
Sx1=V(n*n+(y-1)*n+x+1);
Ry=V(2*n*n+(y-2)*n+x);
Sy1=V(3*n*n+(y)*n+x);
elseif x==n
Rx=V(n*(y-1)+x-1);

```

```

Sx1=0;
Ry=V(2*n*n+(y-2)*n+x);
Sy1=V(3*n*n+(y)*n+x);
elseif y==1
    Rx=V(n*(y-1)+x-1);
    Sx1=V(n*n+(y-1)*n+x+1);
    Ry=0;
    Sy1=V(3*n*n+(y)*n+x);
elseif y==n
    Rx=V(n*(y-1)+x-1);
    Sx1=V(n*n+(y-1)*n+x+1);
    Ry=V(2*n*n+(y-2)*n+x);
    Sy1=0;
else
    Rx=V(n*(y-1)+x-1);
    Sx1=V(n*n+(y-1)*n+x+1);
    Ry=V(2*n*n+(y-2)*n+x);
    Sy1=V(3*n*n+(y)*n+x);
end
Rx1=V(n*(y-1)+x);
Sx=V(n*n+(y-1)*n+x);
Ry1=V(2*n*n+(y-1)*n+x);
Sy=V(3*n*n+(y-1)*n+x);
SE(x,y)=abs(Rx+Rx1)*abs(Rx+Rx1)+abs(Sx+Sx1)*abs(Sx+
Sx1)+abs(Ry+Ry1)*abs(Ry+Ry1)+abs(Sy+Sy1)*abs(Sy+Sy
1);
end
end
figure(3)
[X ,Y]=meshgrid(1:n,1:n);
Plot_Result=surf(X,Y,SE);
f0=f(z2)*100;
cd('C:\Users\jky\Desktop\jky\1');
saveas(Plot_Result, strcat(num2str(f(z2)), 'gain', num2str(realp
art(N(z))), 'w', num2str(imagpart(N(z))), 's', num2str(N(z)),
'.jpg'));
cd('C:\Users\jky\Desktop\couplingconstant');
end
end

```

